The effects of chronic muscle use and disuse on cardiolipin metabolism

Olga Ostojić

A Thesis submitted to the Faculty of Graduate Studies
in Partial Fulfillment of the Requirements for
the Degree of Master of Science

Graduate Programme in Kinesiology and Health Science

York University, Toronto, Ontario

October, 2012

FACULTY OF GRADUATE STUDIES

I recommend that the thesis prepared
under my supervision by

Olga Ostojic

entitled

The effects of chronic muscle use and disuse on cardiolipin metabolism

be accepted in partial fulfillment of the
requirements for the degree of

Master of Science
December 2012

_____
Dr. David Hood, *Supervisor*

Recommendation concurred in by the following Examining Committee

_____
Dr. Olivier Birot, *Chair*

_____
Dr. Katalin Hudak, Outside Member

_____
Dr. David Hood, *Member*

December 2012

YORK

redefine THE **POSSIBLE**.

UNIVERSITÉ
UNIVERSITY

Abstract

Mitochondrial membranes have a diverse structure composed of numerous phospholipids, including cardiolipin (CL). Several processes are required to synthesize and remodel CL. We previously demonstrated that CL content increases with chronic muscle use, and decreases with denervation. To investigate the mechanisms underlying these effects, we measured the mRNA expression of CL metabolism enzymes, including 1) CL synthesis enzymes Cardiolipin synthase (CLS) and CTP:PA-cytidylyltransferase-1 (CDS-1); 2) remodelling enzymes Tafazzin (Taz) and Acyl-CoA:lysocardiolipin acyltransferase-1 (ALCAT1); and 3) outer membrane CL enzymes, Mitochondrial phospholipase D (MitoPLD) and phospholipid scramblase 3 (Plscr3). We found that the transcriptional coactivator PGC-1α regulates the mRNA levels of CDS-1 and ALCAT1, thus playing a role in both CL synthesis and remodelling. We found that all three enzyme categories were altered by our conditions, but unaffected by age, suggesting that chronic muscle use and disuse have divergent influences on the expression of mRNAs encoding enzymes involved in CL metabolism.

Acknowledgments

!!!

Table of Contents

List of Tables

List of Figures

List of abbreviations

ALCAT1	Acyl-CoA:lysocardiolipin acyltransferase-1
AMPK	AMP-activated protein kinase
ANT	Adenine nucleotide translocator
β2M	β2-Microglobulin
CCA	Chronic Contractile Activity
CDS-1	CTP:PA cytidylyltransferase
CDP-DG	Cytidine 5'-diphosphate 1,2-diacyl-sn-glycerol
CL	Cardiolipin
CLS	Cardiolipin Synthase
COX	Cytochrome c oxidase
DAG	Diacylglycerol
DHA	Docosahexaenoic acid
EDL	Extensor digitorum longus
ER	Endoplasmic reticulum
ETC	Electron transport chain
FA	Fatty acid
F344XBN	Fischer 344 X Brown Norway F1 hybrid rat
Gapdh	Glyceraldehyde-3-phosphate dehydrogenase
H+	Hydrogen ions
IMM	Inner mitochondrial membrane
IMF	Intermyofibrillar
MAMs	Mitochondrial-associated membranes
Mfn-2	Mitofusin-2
MitoPLD	Mitochondrial Phospholipase D
MLCL	Monolyso-Cardiolipin

MLCL AT	Monolysocardiolipin acyltransferase
Myc	Myelocytomatosis oncogene
NAO	10-N-Nonyl-3,6-bis(dimethylamino) acridine orange
NRF-1	Nuclear respiratory factor-1
OMM	Outer mitochondrial membrane
PGC-1α	Peroxisome proliferator-activated receptor gamma, coactivator 1 alpha
PA	Phosphatidic acid
Plscr3	Phospholipid scramblase 3
PC	Phosphatidylcholine
PE	Phosphatidylethanolamine
PG	Phosphatidylglycerol
PS	Phosphatidylserine
ROS	Reactive oxygen species
s12	Ribosomal protein 12
SD	Sprague-Dawley
SS	Subsarcolemmal
TA	Tibialis anterior
Taz	Tafazzin
tBid	Truncated B-cell lymphoma 2 interacting domain
TIM	Translocases of the inner mitochondrial membrane
TOM	Translocases of the outer mitochondrial membrane

Literature Review

1.1 The Phospholipid Cardiolipin

1.1.1   Introduction

Since the time of Singer and Nicholson in the 1960s, the fluid mosaic model of membranes has drawn scientists to explore the dynamic world of proteins and phospholipids that encapsulate the cell, as well as the organelles within it. The phospholipid cardiolipin (CL) was first discovered during World War II by a female scientist named Mary Pangborn (100). She initially isolated it from bovine heart tissue, hence the name's cardio- prefix. In mammals, CL is present in all mitochondria-containing tissues, and is most abundantly expressed in the heart. CL is exclusive to both the inner (IMM) and outer mitochondrial membranes (OMM) and has often been called "the glue that holds the electron transport chain (ETC) together" (120). Since then, the phospholipid has been found to play numerous other roles within the cell, including the optimization of ETC function and the execution of mitochondrially-mediated apoptosis.

1.1.2   Structure

CL is a dimeric molecule held together by a glycerol bridge, and is composed of two phosphate heads, four fatty acid (FA) tails and a total of three glycerol groups (66). Due to its dimeric structure and mainly unsaturated FA composition, the molecular structure of CL takes on a cone-like, rather than cylindrical shape, often seen in monomeric phospholipids (Fig. 1A and 1B). It is therefore non-bilayer forming and helps to create the peaks and troughs of mitochondrial cristae (101; 113). It is also important to
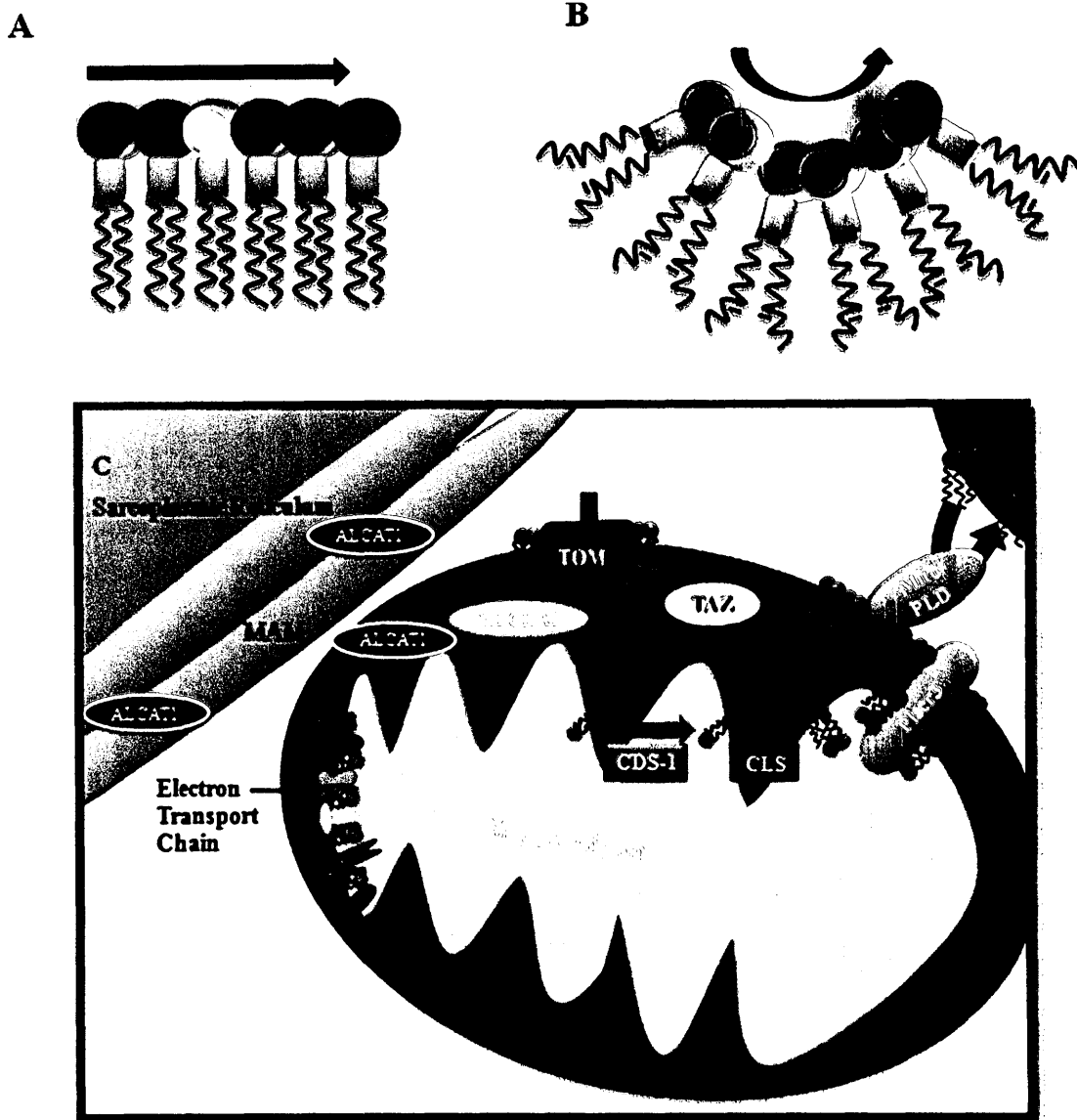
Figure 1. Cardiolipin (CL) structure and localization.
(A) Bilayer forming, monomeric phospholipids, such as phosphatidylcholine and phosphatidylserine. (B) Non-bilayer forming, dimeric phospholipid CL. (C) The localization of CL and its metabolism enzymes. CL *de novo* biosynthesis enzymes are rectangular, while CL transport and remodelling enzymes are oval. MitoPLD, mitochondrial phospholipase D; Plscr3, phospholipid scramblase 3; CDS-1, CTP:PA cytidylyltransferase; PGPS, phosphatidylglycerol-phosphate synthase; CLS, cardiolipin synthase; ALCAT-1, lysocardiolipin acyltransferase; Taz, tafazzin; MLCL AT, monolysocardiolipin acetyltransferase; TOM, translocase of the outer mitochondrial membrane; MAM, mitochondrial-associated membranes.

3

note that the FA composition of CL varies across different species and tissue types. In bacteria and yeast, the CL FA composition varies from 14-18 carbons in length, while oxidative tissue cells in mammals almost exclusively express 18-carbon FA, either the oleic (18:1) or linoleic (18:2) type (44). A prime example of this trend is found in bovine cardiac muscle, where 80% of CL is tetralinoleic (61). The kinks in the unsaturated FAs of tetralinoleic CL contribute to its non-bilayer structure (7). This is particularly beneficial for tissues that contain mitochondria with condensed cristae, such as muscle, which have been shown to have a higher proportion of tetralinoleic CL when compared to non-condensed cristae tissues, such as liver (100). It is also important to note that rats exposed to altered FA diets revealed that CL is most resistant to FA composition alterations, relative to other phospholipids (118). This tightly controlled FA makeup is also crucial for allowing CL to bind to membrane-embedded structures, such as those of the ETC, which helps maintain their structure, alignment and function (100). CL FA alterations have been shown to inhibit CL from enhancing the enzymatic activity of the proteins it binds, thus resulting in a detrimental effect on the cell's function (69; 100).

1.1.3 Function

To call CL the "glue" of the ETC is only appropriate when it is located in the IMM. As we will see, the role that this phospholipid plays in the cell is highly dependent on its location within it.

1.1.3.1 Electron Transport Chain Stabilization

In the IMM, CL ionically binds to, and stabilizes complexes that make up the ETC, including cytochrome c and complexes I, III, IV and V (22). Not only does CL help keep the ETC components aligned to ensure proper electron transfer, it also aids in the stability of dimeric secondary structures found often in the ETC (94; 120). The fourth complex of the ETC is called cytochrome c oxidase (COX), and it binds four CL molecules. COX and CL seem to have a symbiotic relationship; CL increases the enzymatic activity of COX, while COX stabilizes CL's orientation within the membrane (32; 94). CL does not exclusively bind to enzymes present in the ETC. For example, it binds to the adenine nucleotide translocator (ANT), the dimeric structure of which binds six CL molecules so tightly that only denaturing conditions can pry them apart, which results in the complete loss of ANT function (10). Despite the fact that the CL molecules bound to these structures are tetralinoleic, it was shown that neither the hydrogenation of the double bonds, nor the removal of one FA by phospholipase A_2, is able to dissociate CL from ANT, although a reduction in the enzymatic activity of ANT was observed (11).

1.1.3.2 Role in Apoptosis

The location of multiple phospholipids has been found to be crucial for apoptotic signalling within the cell (34; 72). For instance, phosphatidylserine (PS) is found within the plasma membrane, and is transported from the inner to the outer surface of the membrane during apoptosis. Macrophages are then able to recognize the externalized PS,

leading to the consumption of that apoptotic cell via phagocytosis (34). Within the mitochondria, CL is transferred from the IMM to the OMM to act as a binding site for truncated B-cell lymphoma 2 interacting domain (tBid), a proapoptotic protein (81). This interaction allows tBid to localize to the mitochondria and release cytochrome c to induce mitochondrially-mediated apoptosis (22; 37; 81). More specifically, tBid activates the proteins Bax and Bak to form channels on the OMM, through which cytochrome c can be released (81). CL on the IMM also takes part in this process, as CL-cytochrome c bonds must first be broken to release cytochrome c into the intermembrane space (23). This dissociation occurs via the remodelling of CL's FAs. During apoptotic conditions, oleic and linoleic FAs are replaced by longer, more unsaturated FAs (69). This FA composition not only inhibits CL-protein interaction directly, but makes CL more susceptible to damage by reactive oxygen species (ROS), in a process called peroxidation which contributes further to CL-protein dissociation (23; 59; 84). It is therefore not surprising that CL is the only phospholipid that experiences early peroxidation during apoptosis (59).

1.1.4   Localization

1.1.4.1 Inner and Outer Mitochondrial Membranes

While CL is found only in mitochondria, its distribution within the organelle is tightly regulated (Fig. 1C). Originally thought to be exclusive to the IMM, CL has been found to cluster at the mitochondrial contact point regions, where the IMM and OMMs meet, as well as in the OMM itself (7; 60). In studies that split the two membranes, ~90% of CL was found in the IMM, with the remaining ~10% residing in the OMM (39).

1.1.4.2 Phospholipid scramblase 3

The protein family of scramblases is responsible for the bidirectional transport of phospholipids (29). An important member of this protein family, phospholipid scramblase 3 (Plscr3), is embedded within the mitochondrial contact sites and acts to transfer CL between the IMM and OMMs (41; 72). Plscr3 is ATP-independent and is activated both by phosphorylation via Protein Kinase C-δ as well as the binding of calcium (72; 73). As discussed above, the transport of CL to the OMM is an integral part of mitochondrially-mediated apoptosis, making the transporter Plscr3 central to this process (41). While it is known Plscr3 transfers CL in a bidirectional manner, what factors influence the direction of the enzyme's function have been disputed. This debate was brought about when the overexpression of Plscr3 led to increased levels of OMM CL, along with an increased apoptotic susceptibility, while Plscr3 knockdown led to decreased OMM CL and reduced apoptotic susceptibility (73; 114). Which conditions determine the direction of Plscr3's transport of CL remains to be determined. It is also noteworthy that the overexpression of Plscr3 led to decreased mitochondrial respiration and ATP levels, perhaps due to a drop in CL levels in the IMM (73).

1.1.4.3 Mitochondrial Phospholipase D

Mitochondrial phospholipase D (MitoPLD) is the sixth member of the Phospholipase D family (24). It is a dimeric enzyme found on the outer surface of the OMM that acts on adjacent mitochondria to cleave CL into phosphatidic acid (PA), the monomeric form of CL (14; 52). PA on the OMM has been shown to play a role in

7

mitochondrial fission and fusion, either by enhancing fusion via the stabilization of mitofusin-2 (Mfn-2, an OMM fusion protein), or by being converted to diacylglycerol (DAG) by the phosphatase Lipin1, which promotes fission (18; 24; 52). Thus, MitoPLD and Lipin1 have opposing effects on mitochondrial dynamics, and both work through phospholipid messengers (52). MitoPLD's influence on mitochondrial dynamics was first discovered when its overexpression was shown to lead to aggregated mitochondria, while MitoPLD knockdown cells experienced mitochondrial fragmentation. It is important to note that Mfn-2 is necessary to anchor two mitochondria together, only then can MitoPLD exert its effects (24).

1.1.5 Synthesis

Mitochondria contain a mosaic of different phospholipids. Phosphatidylcholine (PC) and phosphatidylethanolamine (PE) are the most abundant. They make up 40% and 30% of the organelle's total phospholipid content, respectively (26). The endoplasmic reticulum (ER, or sarcoplasmic in muscle, SR) is responsible for the production of these two major phospholipids, along with PA (33). The synthesis of CL, however, occurs in the mitochondria and begins like all phospholipid production; through the Kennedy pathway (62). The mitochondria's source of PA comes from two pools: from the ER and from direct production on the OMM (42). The transfer of phospholipids from the ER to the mitochondria is facilitated by structures called mitochondrial-associated membranes, or MAMs (mitochondrial-associated membranes; Fig.1C). Once PA is available, all of the downstream enzymes necessary for its conversion into CL are found in the IMM (35; 50).

1.1.5.1 CDS-1, The Rate Limiting Enzyme

The use of pulse-chase analyses in isolated rat hearts has led to the discovery that CTP:PA cytidylyltransferase (CDS) is the rate-limiting enzyme of *de novo* CL biosynthesis (39). It is responsible for facilitating a reaction that converts PA into cytidine 5'-diphosphate 1,2-diacyl-sn-glycerol (CDP-DG) (100). The mRNA levels of this gene are most abundant in mammalian testes, with relatively low levels in cardiac and skeletal muscle (53; 82). CDS is found on both the matrix side of the IMM, where it contributes to CL production, as well as on the cytoplasmic side of the ER, where it helps produces phosphatidylinositol. There are two known genes that encode CDS in mammals, CDS-1 and CDS-2, but it is important to note that only the mRNA levels of the former match the enzymatic activity of CDS in isolated mitochondrial fractions (53; 82; 96). CDS-1 is therefore thought to play a larger role in the production of CL within the mitochondria, relative to CDS-2 (96).

1.1.5.2 Cardiolipin Synthase, The Final Synthesis Enzyme

The terminal step in the CL *de novo* biosynthesis pathway involves the fusion of phosphatidylglycerol (PG) and CDP-DG, and is executed by the matrix protein cardiolipin synthase (CLS). CLS is located on the inner leaflet of the IMM and its mRNA expression in mammals is most abundant in heart and skeletal muscle (20; 79; 98). It has been shown that the FA composition of the CL precursors PG and CDP-DG are different from those of functional CL molecules (95). This is because CLS has been shown to lack specificity for the FA chains attached to its phospholipid substrates (49). Thus, it was

later discovered that CL FA remodelling follows the production of CL. This dynamic process will be discussed later in more detail. The enzymatic activity of CLS has been shown to be upregulated by thyroid hormone, as well as the presence of the CL molecule itself (17; 99). It was found that the mRNA expression of CLS does not correlate with its enzymatic activity in models of inflammation (80). In striated muscle, however, a correlation was found between CLS mRNA and enzymatic activity (96). It is also noteworthy that increases in CLS activity were shown to upregulate CL content in bacteria (43).

1.1.6 Cardiolipin Remodelling

Since PG and CDP-DG, the precursors of CL, have different FA compositions than CL, post-synthesis remodelling of CL must occur (Fig.2). Like many phospholipids, CL undergoes processes that are part of the Lands' Cycle, a pathway that specifically remodels FA structures on phospholipids (65; 95). A single FA is initially removed from CL to produce monolyso-CL (MLCL), via phospholipase A_2 (14). FAs of desired confirmation are then attached to the MLCL molecule, and this is repeated for all four FAs until optimal FA configuration is achieved (100). As previously stated, CL FA composition is species- and tissue-specific, and mammalian cardiac tissue predominantly expresses tetralinoleic CL, which is optimal for protein-CL binding (63). In mammalian neurons, however, over 100 different CL species exist, perhaps due to less dependence on aerobic respiration in neuronal cells relative to striated muscle (21). The FA composition of CL, and thus its remodelling mechanisms, are crucial determinants of whether CL will be able to bind to, and improve the activities of, the enzymes to which it is bound (11).
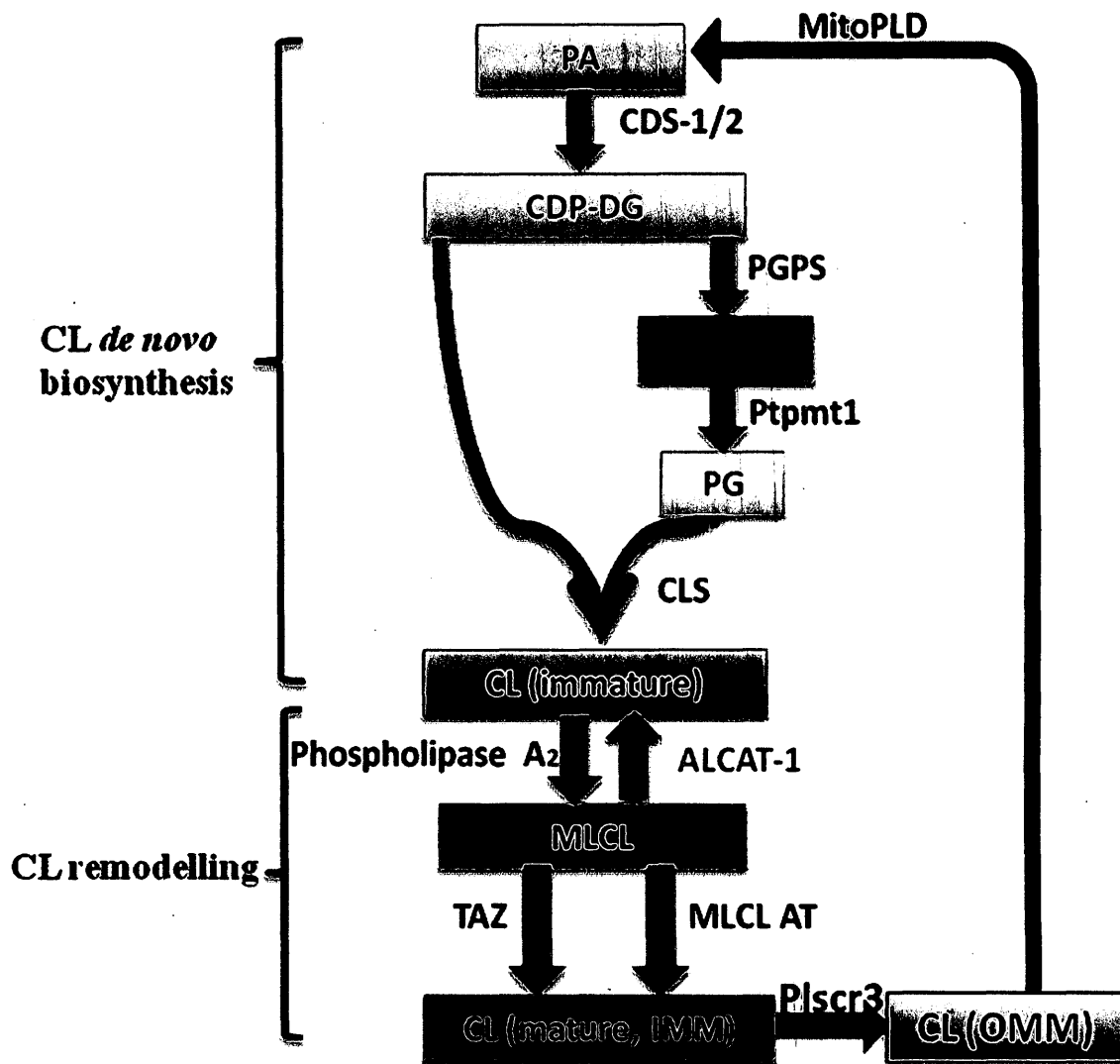
Figure 2. The cardiolipin (CL) metabolism pathway.
MitoPLD, mitochondrial phospholipase D; PA, phosphatidic acid; CDS-1/2, CTP:PA cytidylyltransferase; CDP-DG, cytidine 5'-diphosphate 1,2-diacyl-sn-glycerol; PGPS, phosphatidylglycerol-phosphate synthase; PGP, phosphatidylglycerol phosphate; PGPP, phosphatidylglycerol-phosphate phosphatase; PG, phosphatidylglycerol; CLS, cardiolipin synthase; ALCAT-1, lysocardiolipin acyltransferase; MLCL, monolysocardiolipin; Taz, tafazzin; MLCL AT, monolysocardiolipin acetyltransferase

1.1.6.1 Fatty Acid Peroxidation

The FA composition of CL tends to be unsaturated, which leaves its double bonds vulnerable to damage by ROS via peroxidation (88). CL is at an elevated risk of this damage due to its proximity to the ETC, a major producer of ROS (39). Is has been shown that mitochondrially-mediated production of ROS significantly decreases the enzymatic activities of complexes I, III and IV of the ETC via the peroxidation of CL (86-88). The peroxidation process becomes more likely, and more damaging, as the number of double bonds within the FAs increase. Docosahexaenoic acid (DHA) is a 22 carbon long FA with six double bonds, and is a prime example of a highly peroxidation-sensitive FA that binds to CL. Thus, numerous remodelling enzymes exist to ensure that the CL FA configuration allows optimal enzyme binding as well as maximal peroxidation resistance. Two examples are tafazzin (Taz) and acyl-CoA:lysocardiolipin acyltransferase-1 (ALCAT1).

1.1.6.2 Tafazzin (Taz)

Taz was first identified by an Italian group Bione *et al.* in 1996 (12). In light of their struggle to discover this protein, the group decided to name it after a masochistic, yet lovable, television character called Tafazzi. Taz is perhaps the most studied CL remodelling enzyme in humans, likely because its absence is known to cause Barth Syndrome, an x-linked human disease that is characterized by several myopathies (1; 9; 12). At the molecular level, Taz is located in the intermembrane space and acts as a unique CL remodeler (13). Taz preferentially transfers linoleic FAs onto MLCL in a

CoA-independent manner. That is, it relies on other phospholipids (mainly PC) as FA donors/acceptors, which allow it to create the optimally functioning tetralinoleic CL (119). Taz-deficient neonatal ventricular myocytes have been shown to express decreased levels of CL, as well as lower ATP production (40). Taz KO mice have been generated and found to express increased levels of MLCL among a reduced CL pool, the remainder of which completely lacked tetralinoleic CL and had a higher degree of saturation (1; 51; 106). In addition, these mice mimicked Barth Syndrome patients by exhibiting muscle weakness and cardiomyopathy (9; 106)

1.1.6.3 Acyl-CoA:lysocardiolipin acyltransferase-1 (ALCAT1)

ALCAT1 is responsible for the acyl-CoA-dependent acetylation of MLCL and does not interact with other PLs such as lyso-PC, –PE or –PS (16). The expression of ALCAT1 is most abundant in heart and liver, where it is localized within the ER, MAMs, as well as the mitochondria (16; 69). This localization suggests that ALCAT1 acts on CL residing on the outer surface of the OMM. Unlike Taz, ALCAT1 lacks exclusivity to linoleic FA donor molecules (16). Alas, it is able to replace CL FAs with DHA, which is highly susceptible to peroxidation, and is found to be increasingly bound to CL in pathological conditions (69). DHA CL has been shown to significantly increase during pathological conditions such as heart failure in both humans and rats (96). Overexpression of ALCAT1 has been shown to increase the levels of DHA CL and reduce mitochondrial function, exhibited by increased ROS production, proton leakage and reduced mitochondrial DNA content and Complex I activity (69). The lack of

ALCAT1 has been shown to be beneficial for mitochondrial function, which was demonstrated by the use of ALCAT1 KO mice. These mice exhibited significantly more tetralinoleic-CL and -PG, CL's immediate biosynthetic precursor (58; 69). Accordingly, higher Complex I activity and reduced lipid peroxidation were observed (69). These results, which point to ALCAT1 as a "bad" regulator of CL, are further corroborated by the ability of ALCAT1 to downregulate a monolysocardiolipin acyltransferase (MLCL AT), a "good" CL remodeler that adds only linoleic FA to MLCL (69; 110). ALCAT1 has also been found to be upregulated by ROS, a discovery that is helping elucidate the link between ROS production and mitochondrial dysfunction (69).

1.1.7 Current Research Trends in Cardiolipin

Researchers have generated a Chinese Hamster Ovary cell line that has impaired PGP synthase activity, which leads to significantly decreased levels of CL. As a result of this intervention, mitochondrial swelling, cristae disruption, reduced ATP levels and lower oxygen consumption occurred (85). Complete CL ablation, however, has only been successful in organisms that can survive via anaerobic pathways, such as yeast. Yeast strains with a CLS (Crd1 in yeast) null allele completely lack CL, while PGP synthase (Pgs1 in yeast) null allele cells lack both CL and PG. Crd1-null yeast exhibited defective growth, impaired mitochondrial membrane potential as well as reduced ETC activity and protein import (19; 57; 111). The import of nuclear-encoded proteins into the mitochondria requires translocases of the IMM (TIM) and OMM (TOM) (102). The loss of mitochondrial import in CL-deficient cells has previously been attributed to altered

membrane potential across the IMM. More recently, however, reduced assembly and function of the TIM and TOM complexes have been observed under CL-deficient conditions, hinting that CL may directly influence the integrity of the mitochondrial protein import machinery (64; 109). The production of these cell lines has allowed researchers to explore the effects of CL deficiency, and continues to contribute to the growing body of knowledge on this unique phospholipid.

1.2 Mitochondrial Biogenesis

The plasticity of skeletal muscle is demonstrated by its ability to adapt to conditions of increased metabolic demand, such as exercise. One way that muscle adapts to such stimuli is through mitochondrial biogenesis, or the formation of new mitochondria. This process of organelle biosynthesis requires the coordination of nuclear, cytosolic and mitochondrial functions (47). There are multiple models used in laboratories that induce mitochondrial biogenesis, including treadmill running, overexpression of biogenesis-inducing factors, the use of hormones such as thyroid hormone, as well as the activation of AMP-activated protein kinase (AMPK). It is important to note that there are two subpopulations of mitochondria, both of which adapt to exercise. These are the subsarcolemmal (SS) mitochondria, which are located underneath the muscle's sarcolemma, and the intermyofibrillar (IMF) mitochondria, which are nestled between the myofibrils (25). While 80% of the mitochondrial population is made up of the IMF subfraction, the SS population has been shown to adapt more readily to stimuli such as exercise and states of disease (27; 93).

1.2.1 Signalling pathways overview

Contractile activity in skeletal muscle leads to mitochondrial biogenesis through a series of molecular pathways. One major pathway involved in this process is implemented by intracellular calcium. During muscle contraction, calcium is released from the SR and leads to the increased expression of calcium-induced genes, such as calcium/calmodulin-dependent protein kinases. Another signalling molecule that is activated by exercise is AMPK. Contractile activity in skeletal muscle reduces the ratio of ATP:ADP, and increases the levels of AMP, which allosterically activates AMPK (54). AMPK then translocates into the myonuclei and upregulates the gene expression of proteins involved in mitochondrial biogenesis (56). A third signalling molecule involved in this process is ROS, described below.

1.2.1.1 ROS

Mitochondria are the major producers of ROS in the cell, but ROS can also come from non-mitochondrial sources, such as the flavoprotein oxireductase system, located on the plasma membrane (89). Mitochondrially-produced ROS is generated when an electron is prematurely donated to an oxygen molecule at the ETC. In skeletal muscle, glycolytic muscle fibres have more ROS, relative to their oxidative counterparts and this, in part, is due to the lower expression of ROS scavengers in glycolytic muscles (6). Within these different fibres types, the SS mitochondrial subfraction has been shown to produce more ROS than the IMF fraction (3). Interestingly, ROS molecules were once considered to be solely detrimental, causing damage to mitochondrial DNA and resulting in the

peroxidation of phospholipids such as CL (30; 78). However, moderate levels of ROS, which are produced during exercise, have been shown to have adaptive effects (36; 92). This moderate level of ROS production increases mitochondrial DNA copy number, mitochondrial mass and produces elongation of the mitochondrial reticulum (46; 90). In an effort to elucidate the mechanisms behind these findings, ROS has also been shown to increase peroxisome proliferator-activated receptor gamma, coactivator 1 alpha (PGC-1α) promoter activity as well as the expression of PGC-1α and nuclear respiratory factor-1 (NRF-1) (55; 107).

1.2.2 Transcriptional Coactivator PGC-1α

PGC-1α has often been called the master regulator of mitochondrial biogenesis. The protein expression of PGC-1α was shown to increase with exercise training, as well as with acute exercise followed by recovery, while it decreased with muscle disuse (4; 8; 54). At the molecular level, PGC-1α is a transcriptional coactivator that binds to nuclear transcription factors and influences their interaction with DNA.

1.2.2.1 PGC-1α Overexpression

Muscle-specific overexpression of PGC-1α of an *in vivo* murine model exhibits increased mitochondrial content and improved endurance performance (15). The muscles of these mice also display a switch from glycolytic to more oxidative fibre types and are protected against denervation-induced atrophy (97). This latter effect is likely due to the inhibitory action of PGC-1α on Fox03, a protein involved in muscle atrophy (70; 97).

1.2.2.2 PGC-1α Knockout Mice

The generation of whole-body PGC-1α knockout mice has helped elucidate the effects of this coactivator in an intact physiological setting (71; 112). These mutant mice experience decreased endurance performance and reduced fatigue resistance (38; 68). A decrease in mitochondrial content and respiration was also observed, while the respiration deficit was able to be rescued with training (5). Some exercise physiologists might argue that one of the most intriguing characteristics discovered in the PGC-1α knockout animals is their ability to adapt to exercise training (67; 112). It has been suggested that a compensatory mechanism performed by closely related coactivators, such as PGC-1β, may be at work to induce this effect.

1.3 Chronic Muscle Use

Since the 1960s, it has been known that exercise is able to elicit mitochondrial adaptations in skeletal muscle (45). Each bout of contractile activity leads to the transcriptional activation of both nuclear- and mitochondrially-encoded genes (47). This exercise stimulus leads to the expansion of the mitochondrial network and to the alteration of mitochondrial composition (46). There are multiple rodent models used in research that simulate exercise, including treadmill and voluntary wheel running and chronic contractile activity (CCA).

1.3.1 Endurance Exercise Training

Endurance exercise with progressively increasing intensity has been found to result in mitochondrial biogenesis within 6-8 weeks of training (2; 47; 48). In rodent models, exercise can be administered via voluntary wheel running. This method allows animals to run at their own accord, which means that the exercise duration, frequency the running speed are all intrinsically determined. What is also under independent control is the time of day during which the exercise occurs. This is of particular importance due to the nocturnal activity patterns of rodents. Due to this intrinsic regulation, voluntary wheel running has been proven to elicit less of a stress response when compared to other approaches (31; 103). Two disadvantages of this method include the fact that it results in a lower exercise intensity, and it cannot control for variable exercise performances across animals.

Another common method of exercise involves motorized treadmills, which are known to be of greater intensity when compared to wheel running. The treadmill exposes rodents to a forced running protocol in which the time of day, frequency, duration and progressively increasing intensity of exercise are all predetermined by the researcher (45). The use of air or electrical shocks is often administered to keep animals on track, which has been shown to further increase the stress response (83). A week-long conditioning period is usually used to help animals become accustomed to the treadmills, in an effort to reduce stress levels. Despite this effort, the use of treadmills elicits a greater stress response than the voluntary wheel running approach, one marker of which is increased

adrenal weight (83; 103). The advantage of this technique is that greater adaptations to exercise are observed than with the voluntary running wheel approaches.

1.3.2 Chronic Contractile Activity

CCA is a method used to simulate the repeated contractions performed by skeletal muscle during endurance exercise. This protocol can be used with an animal model, as well as in cell culture (28; 108). *In vivo*, two electrodes are implanted on either side of a nerve, such as the common peroneal nerve, and electrical impulses are sent across the nerve, causing the innervated muscles to contract. In this case, the contracting muscles would be the tibialis anterior (TA) and the extensor digitorum longs (EDL). CCA is of particular benefit because it allows for a comparison to be made between an exercised and non-exercised muscle within the same animal, thus accounting for individual variability (108). Low-frequency stimulation has been shown to induce a training effect within just one week, thus it is also more time-efficient relative to treadmill and voluntary wheel running. CL content has also been shown to increase following just five days of CCA (108). A disadvantage of this protocol is the surgical invasiveness involved with the implantation of the stimulator (108). *In vitro*, the same concept is applied in a cell culture model using skeletal muscle cells (28; 112). A platinum wire electrode is placed on either side of the cell dish and is attached to a stimulator which causes the cells to contract (116). While this protocol induces similar increases in mitochondrial content compared to the *in vivo* model, it is somewhat disadvantageous because these isolated cells cannot experience the whole-body effects that a contracting muscle within an intact organism would (108; 112).

1.4 Chronic Muscle Disuse

The effects of chronic muscle disuse are detrimental to the structure and function of skeletal muscle. The numerous models used in research that simulate muscle disuse include physical inactivity, bed rest, casting, exposure to microgravity, hindlimb suspension in rodents, as well as denervation and aging which are discussed in greater detail below.

1.4.1 Denervation

A denervation protocol involves the removal of a portion of a motor neuron, such as the common peroneal nerve, followed by subsequent analysis of the muscles it once innervated, again the TA and EDL in this case (117). Denervation is known to elicit a condition called sarcopenia, which is characterized by muscle fatigability and atrophy, or muscle fibre loss (4). This process occurs through an upregulation of apoptosis, an increase in protein degradation, and a decrease in the synthesis of newly formed proteins (91). Three days following common peroneal nerve denervation proved to be sufficient in reducing TA muscle mass, mitochondrial content, protein import and respiration levels in both SS and IMF subfractions (4; 104; 117). Following seven days of denervation, ROS production was significantly elevated, while CL levels were shown to decrease within five (104; 117).

1.4.2 Aging

The skeletal muscle of aged mammals exhibits a decreased ability to develop force as well as a reduced muscle mass. Aged muscle is also more susceptible to the development of sarcopenia and has been shown to be less able to adapt to exercise-induced changes, relative to their young counterparts (75). This decreased level of plasticity, however, has been debated. One group found that chronic, low-frequency CCA in rat skeletal muscle elicited the same mitochondrial adaptations in young and aged animals (105). On the other hand, different groups of researchers have found that chronic exercise elicited increased muscle plasticity and fatigue resistance in young, but not aged skeletal muscle (75; 115). It was also found that the activation of exercise-induced kinases was attenuated in aged skeletal muscle and that endurance performance was significantly greater in the young, compared to the old (74; 75). These conflicting findings may be due to different protocol parameters, including rodent age, intensity of exercise and muscle fibres used for analyses (76). Regardless of these discrepancies, rodent models over the age of 26 months have consistently demonstrated attenuated exercise-induced muscle adaptations (74-77; 90; 115). This decreased adaptability of aged skeletal muscle suggests that a larger contractile stimulus is required to elicit the same adaptations (75; 76).

Reference List

1. **Acehan D, Vaz F, Houtkooper RH, James J, Moore V, Tokunaga C, Kulik W, Wansapura J, Toth MJ, Strauss A and Khuchua Z**. Cardiac and skeletal muscle defects in a mouse model of human Barth syndrome. *J Biol Chem* 286: 899-908, 2011.

2. **Adhihetty PJ, Irrcher I, Joseph AM, Ljubicic V and Hood DA**. Plasticity of skeletal muscle mitochondria in response to contractile activity. *Exp Physiol* 88: 99-107, 2003.

3. **Adhihetty PJ, Ljubicic V, Menzies KJ and Hood DA**. Differential susceptibility of subsarcolemmal and intermyofibrillar mitochondria to apoptotic stimuli. *Am J Physiol Cell Physiol* 289: C994-C1001, 2005.

4. **Adhihetty PJ, O'Leary MF, Chabi B, Wicks KL and Hood DA**. Effect of denervation on mitochondrially mediated apoptosis in skeletal muscle. *J Appl Physiol* 102: 1143-1151, 2007.

5. **Adhihetty PJ, Uguccioni G, Leick L, Hidalgo J, Pilegaard H and Hood DA**. The role of PGC-1alpha on mitochondrial function and apoptotic susceptibility in muscle. *Am J Physiol Cell Physiol* 297: C217-C225, 2009.

6. **Anderson EJ and Neufer PD**. Type II skeletal myofibers possess unique properties that potentiate mitochondrial H(2)O(2) generation. *Am J Physiol Cell Physiol* 290: C844-C851, 2006.

7. **Ardail D, Privat JP, Egret-Charlier M, Levrat C, Lerme F and Louisot P**. Mitochondrial contact sites. Lipid composition and dynamics. *J Biol Chem* 265: 18797-18802, 1990.

8. **Baar K, Wende AR, Jones TE, Marison M, Nolte LA, Chen M, Kelly DP and Holloszy JO**. Adaptations of skeletal muscle to exercise: rapid increase in the transcriptional coactivator PGC-1. *FASEB J* 16: 1879-1886, 2002.

9. **Barth PG, Scholte HR, Berden JA, Van der Klei-Van Moorsel JM, Luyt-Houwen IE, Van 't Veer-Korthof ET, Van der Harten JJ and Sobotka-Plojhar MA**. An X-linked mitochondrial disease affecting cardiac muscle, skeletal muscle and neutrophil leucocytes. *J Neurol Sci* 62: 327-355, 1983.

10. **Beyer K and Klingenberg M**. ADP/ATP carrier protein from beef heart mitochondria has high amounts of tightly bound cardiolipin, as revealed by 31P nuclear magnetic resonance. *Biochemistry* 24: 3821-3826, 1985.

11. **Beyer K and Nuscher B**. Specific cardiolipin binding interferes with labeling of sulfhydryl residues in the adenosine diphosphate/adenosine triphosphate carrier protein from beef heart mitochondria. *Biochemistry* 35: 15784-15790, 1996.

12. **Bione S, D'Adamo P, Maestrini E, Gedeon AK, Bolhuis PA and Toniolo D**. A novel X-linked gene, G4.5. is responsible for Barth syndrome. *Nat Genet* 12: 385-389, 1996.

13. **Brandner K, Mick DU, Frazier AE, Taylor RD, Meisinger C and Rehling P**. Taz1, an outer mitochondrial membrane protein, affects stability and assembly of inner membrane protein complexes: implications for Barth Syndrome. *Mol Biol Cell* 16: 5202-5214, 2005.

14. **Cable MB, Jacobus J and Powell GL**. Cardiolipin: a stereospecifically spin-labeled analogue and its specific enzymic hydrolysis. *Proc Natl Acad Sci U S A* 75: 1227-1231, 1978.

15. **Calvo JA, Daniels TG, Wang X, Paul A, Lin J, Spiegelman BM, Stevenson SC and Rangwala SM**. Muscle-specific expression of PPARgamma coactivator-1alpha improves exercise performance and increases peak oxygen uptake. *J Appl Physiol* 104: 1304-1312, 2008.

16. **Cao J, Liu Y, Lockwood J, Burn P and Shi Y**. A novel cardiolipin-remodeling pathway revealed by a gene encoding an endoplasmic reticulum-associated acyl-CoA:lysocardiolipin acyltransferase (ALCAT1) in mouse. *J Biol Chem* 279: 31727-31734, 2004.

17. **Cao SG, Cheng P, Angel A and Hatch GM**. Thyroxine stimulates phosphatidylglycerolphosphate synthase activity in rat heart mitochondria. *Biochim Biophys Acta* 1256: 241-244, 1995.

18. **Cazzolli R, Shemon AN, Fang MQ and Hughes WE**. Phospholipid signalling through phospholipase D and phosphatidic acid. *IUBMB Life* 58: 457-461, 2006.

19. **Chang SC, Heacock PN, Clancey CJ and Dowhan W**. The PEL1 gene (renamed PGS1) encodes the phosphatidylglycero-phosphate synthase of Saccharomyces cerevisiae. *J Biol Chem* 273: 9829-9836, 1998.

20. **Chen D, Zhang XY and Shi Y**. Identification and functional characterization of hCLS1, a human cardiolipin synthase localized in mitochondria. *Biochem J* 398: 169-176, 2006.

21. **Cheng H, Mancuso DJ, Jiang X, Guan S, Yang J, Yang K, Sun G, Gross RW and Han X**. Shotgun lipidomics reveals the temporally dependent, highly diversified cardiolipin profile in the mammalian brain: temporally coordinated postnatal diversification of cardiolipin molecular species with neuronal remodeling. *Biochemistry* 47: 5869-5880, 2008.

22. **Chicco AJ and Sparagna GC**. Role of cardiolipin alterations in mitochondrial dysfunction and disease. *Am J Physiol Cell Physiol* 292: C33-C44, 2007.

23. **Choi SY, Gonzalvez F, Jenkins GM, Slomianny C, Chretien D, Arnoult D, Petit PX and Frohman MA**. Cardiolipin deficiency releases cytochrome c from the inner mitochondrial membrane and accelerates stimuli-elicited apoptosis. *Cell Death Differ* 14: 597-606, 2007.

24. **Choi SY, Huang P, Jenkins GM, Chan DC, Schiller J and Frohman MA**. A common lipid links Mfn-mediated mitochondrial fusion and SNARE-regulated exocytosis. *Nat Cell Biol* 8: 1255-1262, 2006.

25. **Cogswell AM, Stevens RJ and Hood DA**. Properties of skeletal muscle mitochondria isolated from subsarcolemmal and intermyofibrillar regions. *Am J Physiol* 264: C383-C389, 1993.

26. **Colbeau A, Nachbaur J and Vignais PM**. Enzymic characterization and lipid composition of rat liver subcellular membranes. *Biochim Biophys Acta* 249: 462-492, 1971.

27. **Connor MK, Bezborodova O, Escobar CP and Hood DA**. Effect of contractile activity on protein turnover in skeletal muscle mitochondrial subfractions. *J Appl Physiol* 88: 1601-1606, 2000.

28. **Connor MK, Irrcher I and Hood DA**. Contractile activity-induced transcriptional activation of cytochrome C involves Sp1 and is proportional to mitochondrial ATP synthesis in C2C12 muscle cells. *J Biol Chem* 276: 15898-15904, 2001.

29. **Daleke DL and Lyles JV**. Identification and purification of aminophospholipid flippases. *Biochim Biophys Acta* 1486: 108-127, 2000.

30. **Davies KJ, Quintanilha AT, Brooks GA and Packer L**. Free radicals and tissue damage produced by exercise. *Biochem Biophys Res Commun* 107: 1198-1205, 1982.

31. **De Bono JP, Adlam D, Paterson DJ and Channon KM**. Novel quantitative phenotypes of exercise training in mouse models. *Am J Physiol Regul Integr Comp Physiol* 290: R926-R934, 2006.

32. **de KB and Cullis PR**. Cytochrome c specifically induces non-bilayer structures in cardiolipin-containing model membranes. *Biochim Biophys Acta* 602: 477-490, 1980.

33. **Dowhan W**. Molecular basis for membrane phospholipid diversity: why are there so many lipids? *Annu Rev Biochem* 66: 199-232, 1997.

34. **Fadok VA, Voelker DR, Campbell PA, Cohen JJ, Bratton DL and Henson PM**. Exposure of phosphatidylserine on the surface of apoptotic lymphocytes triggers specific recognition and removal by macrophages. *J Immunol* 148: 2207-2216, 1992.

35. **Gaigg B, Simbeni R, Hrastnik C, Paltauf F and Daum G**. Characterization of a microsomal subfraction associated with mitochondria of the yeast, Saccharomyces cerevisiae. Involvement in synthesis and import of phospholipids into mitochondria. *Biochim Biophys Acta* 1234: 214-220, 1995.

36. **Gomez-Cabrera MC, Borras C, Pallardo FV, Sastre J, Ji LL and Vina J**. Decreasing xanthine oxidase-mediated oxidative stress prevents useful cellular adaptations to exercise in rats. *J Physiol* 567: 113-120, 2005.

37. **Gonzalvez F, Pariselli F, Dupaigne P, Budihardjo I, Lutter M, Antonsson B, Diolez P, Manon S, Martinou JC, Goubern M, Wang X, Bernard S and Petit PX**. tBid interaction with cardiolipin primarily orchestrates mitochondrial dysfunctions and subsequently activates Bax and Bak. *Cell Death Differ* 12: 614-626, 2005.

38. **Handschin C, Chin S, Li P, Liu F, Maratos-Flier E, Lebrasseur NK, Yan Z and Spiegelman BM**. Skeletal muscle fiber-type switching, exercise intolerance, and myopathy in PGC-1alpha muscle-specific knock-out animals. *J Biol Chem* 282: 30014-30021, 2007.

39. **Hatch GM**. Cardiolipin biosynthesis in the isolated heart. *Biochem J* 297 (Pt 1): 201-208, 1994.

40. **He Q**. Tafazzin knockdown causes hypertrophy of neonatal ventricular myocytes. *Am J Physiol Heart Circ Physiol* 299: H210-H216, 2010.

41. **He Y, Liu J, Grossman D, Durrant D, Sweatman T, Lothstein L, Epand RF, Epand RM and Lee RM**. Phosphorylation of mitochondrial phospholipid scramblase 3 by protein kinase C-delta induces its activation and facilitates mitochondrial targeting of tBid. *J Cell Biochem* 101: 1210-1221, 2007.

42. **Hesler CB, Carroll MA and Haldar D**. The topography of glycerophosphate acyltransferase in the transverse plane of the mitochondrial outer membrane. *J Biol Chem* 260: 7452-7456, 1985.

43. **Hiraoka S, Matsuzaki H and Shibuya I**. Active increase in cardiolipin synthesis in the stationary growth phase and its physiological significance in Escherichia coli. *FEBS Lett* 336: 221-224, 1993.

44. **Hoch FL**. Cardiolipins and biomembrane function. *Biochim Biophys Acta* 1113: 71-133, 1992.

45. **Holloszy JO**. Biochemical adaptations in muscle. Effects of exercise on mitochondrial oxygen uptake and respiratory enzyme activity in skeletal muscle. *J Biol Chem* 242: 2278-2282, 1967.

46. **Hood DA**. Mechanisms of exercise-induced mitochondrial biogenesis in skeletal muscle. *Appl Physiol Nutr Metab* 34: 465-472, 2009.

47. **Hood DA**. Invited Review: contractile activity-induced mitochondrial biogenesis in skeletal muscle. *J Appl Physiol* 90: 1137-1157, 2001.

48. **Hood DA, Irrcher I, Ljubicic V and Joseph AM**. Coordination of metabolic plasticity in skeletal muscle. *J Exp Biol* 209: 2265-2275, 2006.

49. **Hostetler KY, Galesloot JM, Boer P and Van Den BH**. Further studies on the formation of cardiolipin and phosphatidylglycerol in rat liver mitochondria. Effect of divalent cations and the fatty acid composition of CDP-diglyceride. *Biochim Biophys Acta* 380: 382-389, 1975.

50. **Hostetler KY and Van Den BH**. Subcellular and submitochondrial localization of the biosynthesis of cardiolipin and related phospholipids in rat liver. *Biochim Biophys Acta* 260: 380-386, 1972.

51. **Houtkooper RH, Rodenburg RJ, Thiels C, van LH, Stet F, Poll-The BT, Stone JE, Steward CG, Wanders RJ, Smeitink J, Kulik W and Vaz FM**. Cardiolipin and monolysocardiolipin analysis in fibroblasts, lymphocytes, and tissues using high-performance liquid chromatography-mass spectrometry as a diagnostic test for Barth syndrome. *Anal Biochem* 387: 230-237, 2009.

52. **Huang H, Gao Q, Peng X, Choi SY, Sarma K, Ren H, Morris AJ and Frohman MA**. piRNA-associated germline nuage formation and spermatogenesis require MitoPLD profusogenic mitochondrial-surface lipid signaling. *Dev Cell* 20: 376-387, 2011.

53. **Inglis-Broadgate SL, Ocaka L, Banerjee R, Gaasenbeek M, Chapple JP, Cheetham ME, Clark BJ, Hunt DM and Halford S.** Isolation and characterization of murine Cds (CDP-diacylglycerol synthase) 1 and 2. *Gene* 356: 19-31, 2005.

54. **Irrcher I, Adhihetty PJ, Sheehan T, Joseph AM and Hood DA.** PPARgamma coactivator-1alpha expression during thyroid hormone- and contractile activity-induced mitochondrial adaptations. *Am J Physiol Cell Physiol* 284: C1669-C1677, 2003.

55. **Irrcher I, Ljubicic V and Hood DA.** Interactions between ROS and AMP kinase activity in the regulation of PGC-1alpha transcription in skeletal muscle cells. *Am J Physiol Cell Physiol* 296: C116-C123, 2009.

56. **Irrcher I, Ljubicic V, Kirwan AF and Hood DA.** AMP-activated protein kinase-regulated activation of the PGC-1alpha promoter in skeletal muscle cells. *PLoS One* 3: e3614, 2008.

57. **Jiang F, Rizavi HS and Greenberg ML.** Cardiolipin is not essential for the growth of Saccharomyces cerevisiae on fermentable or non-fermentable carbon sources. *Mol Microbiol* 26: 481-491, 1997.

58. **Jiang F, Ryan MT, Schlame M, Zhao M, Gu Z, Klingenberg M, Pfanner N and Greenberg ML.** Absence of cardiolipin in the crd1 null mutant results in decreased mitochondrial membrane potential and reduced mitochondrial function. *J Biol Chem* 275: 22387-22394, 2000.

59. **Kagan VE, Bayir HA, Belikova NA, Kapralov O, Tyurina YY, Tyurin VA, Jiang J, Stoyanovsky DA, Wipf P, Kochanek PM, Greenberger JS, Pitt B, Shvedova AA and Borisenko G.** Cytochrome c/cardiolipin relations in mitochondria: a kiss of death. *Free Radic Biol Med* 46: 1439-1453, 2009.

60. **Kagan VE, Tyurin VA, Jiang J, Tyurina YY, Ritov VB, Amoscato AA, Osipov AN, Belikova NA, Kapralov AA, Kini V, Vlasova II, Zhao Q, Zou M, Di P, Svistunenko DA, Kurnikov IV and Borisenko GG.** Cytochrome c acts as a cardiolipin oxygenase required for release of proapoptotic factors. *Nat Chem Biol* 1: 223-232, 2005.

61. **Keenan TW, Awasthi YC and Crane FL.** Cardiolipin from beef heart mitochondria: fatty acid positioning an molecular species distribution. *Biochem Biophys Res Commun* 40: 1102-1109, 1970.

62. **KENNEDY EP and WEISS SB.** The function of cytidine coenzymes in the biosynthesis of phospholipides. *J Biol Chem* 222: 193-214, 1956.

63. **Kiebish MA, Bell R, Yang K, Phan T, Zhao Z, Ames W, Seyfried TN, Gross RW, Chuang JH and Han X.** Dynamic simulation of cardiolipin remodeling: greasing the wheels for an interpretative approach to lipidomics. *J Lipid Res* 51: 2153-2170, 2010.

64. **Kutik S, Rissler M, Guan XL, Guiard B, Shui G, Gebert N, Heacock PN, Rehling P, Dowhan W, Wenk MR, Pfanner N and Wiedemann N.** The translocator maintenance protein Tam41 is required for mitochondrial cardiolipin biosynthesis. *J Cell Biol* 183: 1213-1221, 2008.

65. **LANDS WE.** Metabolism of glycerolipides; a comparison of lecithin and triglyceride synthesis. *J Biol Chem* 231: 883-888, 1958.

66. **LECOCQ J and BALLOU CE.** ON THE STRUCTURE OF CARDIOLIPIN. *Biochemistry* 3: 976-980, 1964.

67. **Leick L, Wojtaszewski JF, Johansen ST, Kiilerich K, Comes G, Hellsten Y, Hidalgo J and Pilegaard H.** PGC-1alpha is not mandatory for exercise- and training-induced adaptive gene responses in mouse skeletal muscle. *Am J Physiol Endocrinol Metab* 294: E463-E474, 2008.

68. **Leone TC, Lehman JJ, Finck BN, Schaeffer PJ, Wende AR, Boudina S, Courtois M, Wozniak DF, Sambandam N, Bernal-Mizrachi C, Chen Z, Holloszy JO, Medeiros DM, Schmidt RE, Saffitz JE, Abel ED, Semenkovich CF and Kelly DP.** PGC-1alpha deficiency causes multi-system energy metabolic derangements: muscle dysfunction, abnormal weight control and hepatic steatosis. *PLoS Biol* 3: e101, 2005.

69. **Li J, Romestaing C, Han X, Li Y, Hao X, Wu Y, Sun C, Liu X, Jefferson LS, Xiong J, Lanoue KF, Chang Z, Lynch CJ, Wang H and Shi Y.** Cardiolipin

remodeling by ALCAT1 links oxidative stress and mitochondrial dysfunction to obesity. *Cell Metab* 12: 154-165, 2010.

70. **Lin J, Wu H, Tarr PT, Zhang CY, Wu Z, Boss O, Michael LF, Puigserver P, Isotani E, Olson EN, Lowell BB, Bassel-Duby R and Spiegelman BM.** Transcriptional co-activator PGC-1 alpha drives the formation of slow-twitch muscle fibres. *Nature* 418: 797-801, 2002.

71. **Lin J, Wu PH, Tarr PT, Lindenberg KS, St-Pierre J, Zhang CY, Mootha VK, Jager S, Vianna CR, Reznick RM, Cui L, Manieri M, Donovan MX, Wu Z, Cooper MP, Fan MC, Rohas LM, Zavacki AM, Cinti S, Shulman GI, Lowell BB, Krainc D and Spiegelman BM.** Defects in adaptive energy metabolism with CNS-linked hyperactivity in PGC-1alpha null mice. *Cell* 119: 121-135, 2004.

72. **Liu J, Chen J, Dai Q and Lee RM.** Phospholipid scramblase 3 is the mitochondrial target of protein kinase C delta-induced apoptosis. *Cancer Res* 63: 1153-1156, 2003.

73. **Liu J, Dai Q, Chen J, Durrant D, Freeman A, Liu T, Grossman D and Lee RM.** Phospholipid scramblase 3 controls mitochondrial structure, function, and apoptotic response. *Mol Cancer Res* 1: 892-902, 2003.

74. **Ljubicic V and Hood DA.** Diminished contraction-induced intracellular signaling towards mitochondrial biogenesis in aged skeletal muscle. *Aging Cell* 8: 394-404, 2009.

75. **Ljubicic V, Joseph AM, Adhihetty PJ, Huang JH, Saleem A, Uguccioni G and Hood DA.** Molecular basis for an attenuated mitochondrial adaptive plasticity in aged skeletal muscle. *Aging (Albany NY)* 1: 818-830, 2009.

76. **Ljubicic V, Joseph AM, Saleem A, Uguccioni G, Collu-Marchese M, Lai RY, Nguyen LM and Hood DA.** Transcriptional and post-transcriptional regulation of mitochondrial biogenesis in skeletal muscle: effects of exercise and aging. *Biochim Biophys Acta* 1800: 223-234, 2010.

77. **Ljubicic V, Menzies KJ and Hood DA.** Mitochondrial dysfunction is associated with a pro-apoptotic cellular environment in senescent cardiac muscle. *Mech Ageing Dev* 131: 79-88, 2010.

78. **Loeb LA, Wallace DC and Martin GM.** The mitochondrial theory of aging and its relationship to reactive oxygen species damage and somatic mtDNA mutations. *Proc Natl Acad Sci U S A* 102: 18769-18770, 2005.

79. **Lu B, Xu FY, Jiang YJ, Choy PC, Hatch GM, Grunfeld C and Feingold KR.** Cloning and characterization of a cDNA encoding human cardiolipin synthase (hCLS1). *J Lipid Res* 47: 1140-1145, 2006.

80. **Lu B, Xu FY, Taylor WA, Feingold KR and Hatch GM.** Cardiolipin synthase-1 mRNA expression does not correlate with endogenous cardiolipin synthase enzyme activity in vitro and in vivo in mammalian lipopolysaccharide models of inflammation. *Inflammation* 34: 247-254, 2011.

81. **Lutter M, Fang M, Luo X, Nishijima M, Xie X and Wang X.** Cardiolipin provides specificity for targeting of tBid to mitochondria. *Nat Cell Biol* 2: 754-761, 2000.

82. **Mercade A, Sanchez A and Folch JM.** Characterization and physical mapping of the porcine CDS1 and CDS2 genes. *Anim Biotechnol* 18: 23-35, 2007.

83. **Moraska A, Deak T, Spencer RL, Roth D and Fleshner M.** Treadmill running produces both positive and negative physiological adaptations in Sprague-Dawley rats. *Am J Physiol Regul Integr Comp Physiol* 279: R1321-R1329, 2000.

84. **Nomura K, Imai H, Koumura T, Kobayashi T and Nakagawa Y.** Mitochondrial phospholipid hydroperoxide glutathione peroxidase inhibits the release of cytochrome c from mitochondria by suppressing the peroxidation of cardiolipin in hypoglycaemia-induced apoptosis. *Biochem J* 351: 183-193, 2000.

85. **Ohtsuka T, Nishijima M, Suzuki K and Akamatsu Y.** Mitochondrial dysfunction of a cultured Chinese hamster ovary cell mutant deficient in cardiolipin. *J Biol Chem* 268: 22914-22919, 1993.

86. **Paradies G, Petrosillo G, Pistolese M and Ruggiero FM.** The effect of reactive oxygen species generated from the mitochondrial electron transport chain on the cytochrome c oxidase activity and on the cardiolipin content in bovine heart submitochondrial particles. *FEBS Lett* 466: 323-326, 2000.

87. **Paradies G, Petrosillo G, Pistolese M and Ruggiero FM**. Reactive oxygen species generated by the mitochondrial respiratory chain affect the complex III activity via cardiolipin peroxidation in beef-heart submitochondrial particles. *Mitochondrion* 1: 151-159, 2001.

88. **Paradies G, Petrosillo G, Pistolese M and Ruggiero FM**. Reactive oxygen species affect mitochondrial electron transport complex I activity through oxidative cardiolipin damage. *Gene* 286: 135-141, 2002.

89. **Pattwell DM, McArdle A, Morgan JE, Patridge TA and Jackson MJ**. Release of reactive oxygen and nitrogen species from contracting skeletal muscle cells. *Free Radic Biol Med* 37: 1064-1072, 2004.

90. **Pesce V, Cormio A, Fracasso F, Lezza AM, Cantatore P and Gadaleta MN**. Age-related changes of mitochondrial DNA content and mitochondrial genotypic and phenotypic alterations in rat hind-limb skeletal muscles. *J Gerontol A Biol Sci Med Sci* 60: 715-723, 2005.

91. **Phillips SM, Glover EI and Rennie MJ**. Alterations of protein turnover underlying disuse atrophy in human skeletal muscle. *J Appl Physiol* 107: 645-654, 2009.

92. **Ristow M, Zarse K, Oberbach A, Kloting N, Birringer M, Kiehntopf M, Stumvoll M, Kahn CR and Bluher M**. Antioxidants prevent health-promoting effects of physical exercise in humans. *Proc Natl Acad Sci U S A* 106: 8665-8670, 2009.

93. **Ritov VB, Menshikova EV, He J, Ferrell RE, Goodpaster BH and Kelley DE**. Deficiency of subsarcolemmal mitochondria in obesity and type 2 diabetes. *Diabetes* 54: 8-14, 2005.

94. **Robinson NC, Zborowski J and Talbert LH**. Cardiolipin-depleted bovine heart cytochrome c oxidase: binding stoichiometry and affinity for cardiolipin derivatives. *Biochemistry* 29: 8962-8969, 1990.

95. **Rustow B, Schlame M, Rabe H, Reichmann G and Kunze D**. Species pattern of phosphatidic acid, diacylglycerol, CDP-diacylglycerol and

phosphatidylglycerol synthesized de novo in rat liver mitochondria. *Biochim Biophys Acta* 1002: 261-263, 1989.

96. **Saini-Chohan HK, Holmes MG, Chicco AJ, Taylor WA, Moore RL, McCune SA, Hickson-Bick DL, Hatch GM and Sparagna GC.** Cardiolipin biosynthesis and remodeling enzymes are altered during development of heart failure. *J Lipid Res* 50: 1600-1608, 2009.

97. **Sandri M, Lin J, Handschin C, Yang W, Arany ZP, Lecker SH, Goldberg AL and Spiegelman BM.** PGC-1alpha protects skeletal muscle from atrophy by suppressing FoxO3 action and atrophy-specific gene transcription. *Proc Natl Acad Sci U S A* 103: 16260-16265, 2006.

98. **Schlame M and Haldar D.** Cardiolipin is synthesized on the matrix side of the inner membrane in rat liver mitochondria. *J Biol Chem* 268: 74-79, 1993.

99. **Schlame M and Hostetler KY.** Solubilization, purification, and characterization of cardiolipin synthase from rat liver mitochondria. Demonstration of its phospholipid requirement. *J Biol Chem* 266: 22398-22403, 1991.

100. **Schlame M, Rua D and Greenberg ML.** The biosynthesis and functional role of cardiolipin. *Prog Lipid Res* 39: 257-288, 2000.

101. **Schlame M, Shanske S, Doty S, Konig T, Sculco T, DiMauro S and Blanck TJ.** Microanalysis of cardiolipin in small biopsies including skeletal muscle from patients with mitochondrial disease. *J Lipid Res* 40: 1585-1592, 1999.

102. **Schmidt O, Pfanner N and Meisinger C.** Mitochondrial protein import: from proteomics to functional mechanisms. *Nat Rev Mol Cell Biol* 11: 655-667, 2010.

103. **Servais S, Couturier K, Koubi H, Rouanet JL, Desplanches D, Sornay-Mayet MH, Sempore B, Lavoie JM and Favier R.** Effect of voluntary exercise on H2O2 release by subsarcolemmal and intermyofibrillar mitochondria. *Free Radic Biol Med* 35: 24-32, 2003.

104. **Singh K and Hood DA.** Effect of denervation-induced muscle disuse on mitochondrial protein import. *Am J Physiol Cell Physiol* 300: C138-C145, 2011.

105. **Skorjanc D, Traub I and Pette D**. Identical responses of fast muscle to sustained activity by low-frequency stimulation in young and aging rats. *J Appl Physiol* 85: 437-441, 1998.

106. **Soustek MS, Falk DJ, Mah CS, Toth MJ, Schlame M, Lewin AS and Byrne BJ**. Characterization of a transgenic short hairpin RNA-induced murine model of Tafazzin deficiency. *Hum Gene Ther* 22: 865-871, 2011.

107. **Suliman HB, Carraway MS, Welty-Wolf KE, Whorton AR and Piantadosi CA**. Lipopolysaccharide stimulates mitochondrial biogenesis via activation of nuclear respiratory factor-1. *J Biol Chem* 278: 41510-41518, 2003.

108. **Takahashi M and Hood DA**. Chronic stimulation-induced changes in mitochondria and performance in rat skeletal muscle. *J Appl Physiol* 74: 934-941, 1993.

109. **Tamura Y, Endo T, Iijima M and Sesaki H**. Ups1p and Ups2p antagonistically regulate cardiolipin metabolism in mitochondria. *J Cell Biol* 185: 1029-1045, 2009.

110. **Taylor WA and Hatch GM**. Purification and characterization of monolysocardiolipin acyltransferase from pig liver mitochondria. *J Biol Chem* 278: 12716-12721, 2003.

111. **Tuller G, Hrastnik C, Achleitner G, Schiefthaler U, Klein F and Daum G**. YDL142c encodes cardiolipin synthase (Cls1p) and is non-essential for aerobic growth of Saccharomyces cerevisiae. *FEBS Lett* 421: 15-18, 1998.

112. **Uguccioni G and Hood DA**. The importance of PGC-1alpha in contractile activity-induced mitochondrial adaptations. *Am J Physiol Endocrinol Metab* 300: E361-E371, 2011.

113. **van den Brink-van der Laan, Killian JA and de KB**. Nonbilayer lipids affect peripheral and integral membrane proteins via changes in the lateral pressure profile. *Biochim Biophys Acta* 1666: 275-288, 2004.

114. **Van Q, Liu J, Lu B, Feingold KR, Shi Y, Lee RM and Hatch GM.** Phospholipid scramblase-3 regulates cardiolipin de novo biosynthesis and its resynthesis in growing HeLa cells. *Biochem J* 401: 103-109, 2007.

115. **Walters TJ, Sweeney HL and Farrar RP.** Influence of electrical stimulation on a fast-twitch muscle in aging rats. *J Appl Physiol* 71: 1921-1928, 1991.

116. **Wehrle U, Dusterhoft S and Pette D.** Effects of chronic electrical stimulation on myosin heavy chain expression in satellite cell cultures derived from rat muscles of different fiber-type composition. *Differentiation* 58: 37-46, 1994.

117. **Wicks KL and Hood DA.** Mitochondrial adaptations in denervated muscle: relationship to muscle performance. *Am J Physiol* 260: C841-C850, 1991.

118. **Wolff RL.** Structural importance of the cis-5 ethylenic bond in the endogenous desaturation product of dietary elaidic acid, cis-5,trans-9 18:2 acid, for the acylation of rat mitochondria phosphatidylinositol. *Lipids* 30: 893-898, 1995.

119. **Xu Y, Malhotra A, Ren M and Schlame M.** The enzymatic function of tafazzin. *J Biol Chem* 281: 39217-39224, 2006.

120. **Zhang M, Mileykovskaya E and Dowhan W.** Gluing the respiratory chain together. Cardiolipin is required for supercomplex formation in the inner mitochondrial membrane. *J Biol Chem* 277: 43553-43556, 2002.

Manuscript Author Contributions

Olga Ostojic performed all of the experiments, analyzed and interpreted all of the data, and wrote the manuscript.

Michael F.N. O'Leary performed the chronic contractile activity and denervation surgeries for both aged animal studies.

Kaustabh Singh performed denervation surgeries in young animals.

Dr. Keir J. Menzies performed all flow cytometry experiments.

Dr. David A. Hood designed and supervised this project. He is the principal investigator.

The effects of chronic muscle use and disuse on cardiolipin metabolism

Olga Ostojić, Michael F.N. O'Leary, Kaustabh Singh, Keir J. Menzies, Anna Vainshtein
and David A. Hood

School of Kinesiology and Health Science, York University
Toronto, Ontario, M3J 1P3, Canada

Muscle Health Research Centre, York University
Toronto, Ontario, M3J 1P3, Canada

To whom correspondence should be addressed: David A. Hood
School of Kinesiology
York University, Toronto, ON
M3J 1P3, Canada
Tel: (416) 736-2100 ext. 66640
Fax: (416) 736-5698
Email: dhood@yorku.ca

Abstract

Cardiolipin (CL) is a phospholipid that maintains the integrity of mitochondrial membranes. We previously demonstrated that CL content increases with chronic muscle use, and decreases with denervation-induced disuse. To investigate the underlying mechanisms, we measured the mRNA expression of 1) CL synthesis enzymes cardiolipin synthase (CLS) and CTP:PA-cytidylyltransferase-1 (CDS-1), 2) remodelling enzymes tafazzin (Taz) and acyl-CoA:lysocardiolipin acyltransferase-1 (ALCAT1), and 3) outer membrane CL enzymes, mitochondrial phospholipase D (MitoPLD) and phospholipid scramblase 3 (Plscr3), during chronic contractile activity (CCA)-induced mitochondrial biogenesis and denervation. With CCA, CDS-1 expression increased by 128%, parelleling CL levels. Surprisingly, denervation also led to large increases in CDS-1 and CLS, despite a decrease in mitochondria, possibly due to a compensatory mechanism to restore lost CL. ALCAT1 decreased by 32% with CCA, but increased by 290% following denervation, indicating that both CCA and denervation alter CL remodelling. CCA and denervation also elicited 60-90% increases in Plscr3, likely to facilitate CL movement to the outer membrane. The expression of these genes was not affected by aging, but changes due to CCA and denervation were attenuated compared to young animals. The absence of PGC-1α in knockout animals led to a decrease in CDS-1 and an increase in ALCAT1 mRNA levels, implicating PGC-1α in regulating both CL synthesis and remodelling. These data suggest that chronic muscle use and disuse modify the expression of mRNAs encoding CL metabolism enzymes. Our data also illustrate, for the first time, that PGC-1α regulates the CL metabolism pathway in muscle.

Introduction

The membranes of mitochondria have a diverse structure consisting of many molecules including cholesterol, proteins and phospholipids. The most abundant structures are the phospholipids, which further contribute to the diversity of membranes through their varied forms. Cardiolipin (CL) is a phospholipid exclusive to the mitochondria, with 90% of it localizing in the inner mitochondrial membrane (IMM), with the remaining 10% on the outer mitochondrial membrane (OMM) (13). CL exists as a dimer and is composed of four fatty acid (FA) chains which must be dynamically transferred and remodelled to ensure proper membrane configuration (18). The majority of these FA molecules are unsaturated, making them highly susceptible to peroxidation via reactive oxygen species (ROS). CL also binds to components of the electron transport chain (ETC), a major producer of ROS, and is therefore at even greater risk of peroxidation (19). When CL is peroxidized, proton leak is increased across the IMM, thus inhibiting energy production and leading to pathology (14).

A complex molecular pathway is involved in synthesizing and ensuring proper CL structure. Cardiolipin synthase (CLS) is a key enzyme involved in the *de novo* biosynthesis of immature CL, which occurs on the inner leaflet of the IMM (6). Another crucial enzyme involved in this pathway is CTP:PA cytidylyltransferase (CDS-1), the rate limiting step of this biosynthesis process (13). In order to function optimally, immature CL must have its FAs remodelled into a mature form. Two key enzymes involved in this are tafazzin (Taz) and acyl-CoA:lysocardiolipin acyltransferase-1 (ALCAT1). Taz remodels the FAs of CL to create a mature CL molecule (4), while ALCAT1 converts the

FAs back to the immature form (14). CL can also be transferred between the IMM and OMM by the membrane-embedded enzyme phospholipid scramblase-3 (Plscr3) (21). This is critical, as the location of CL has been found to influence its cellular role (12). IMM CL that is bound to the ETC complexes helps to stabilize and align them to ensure proper electron transfer (7), while CL that is located on the OMM aids in the assembly of import machinery, and acts as a binding site for tBid, which triggers apoptosis (11; 12). OMM CL is also at risk of being cleaved and converted to phosphatidic acid (PA) by mitochondrial phospholipase D (MitoPLD), which acts only on adjacent mitochondria (8). MitoPLD, therefore, is of particular importance, as it has the ability to mediate the amount of CL that resides on the OMM.

The synthesis and remodelling of CL is crucial for the integrity of the mitochondrial membrane and overall functioning of the organelle. We have previously shown that chronic contractile activity (CCA), a form of muscle use, elicits a significant increase in CL content (20). In contrast, denervation, a form of muscle disuse, significantly decreases CL concentration within muscle (22). The mechanisms underlying these changes have yet to be examined. Thus, the purpose of this study is to examine the adaptations of the enzymes of the CL metabolism pathway during changes in mitochondrial biogenesis. We set out to analyze the expression of the six aforementioned enzymes in response to conditions of chronic muscle use and disuse, and the effect of aging. Further, since many mitochondrial proteins are regulated by the transcriptional coactivator PGC-1α, we also evaluated the role of this protein in the regulation of CL metabolism enzymes. We hypothesized that the gene expressions of the enzymes

41

involved in CL biosynthesis and remodelling would increase with CCA and decrease with denervation and PCG-1α knockout conditions. We also predicted that the expression of enzymes that reduce CL content or function would be downregulated with CCA and increased with denervation and PCG-1α knockdown. The combined effects of these changes would result in increased CL content with CCA, and decreased content in denervated and PCG-1α knockout rodents. This could contribute to the expansion and degradation of mitochondrial membranes as alterations in mitochondrial content occur.

Methods

Animals. Male Sprague-Dawley (SD; Charles River, St. Constant, QC, Canada) rats were purchased at six-months of age. Male Fischer 344 X Brown Norway (F344XBN; National Institute on Aging, Bethesda, MD, USA) F1 hybrid rats were divided into one of two groups depending on age: six-months (young) or 33-months old (aged). One set of young and aged rats were designated for our CCA protocol (n=10 for both young and aged), while a separate set was used for denervation (n=8 for both young and aged). The generation of PGC-1α knockout mice used were as was previously described (15), and are bred in our facility. Offspring were genotyped by crude DNA extraction from ear clippings. DNA was combined with DNA *Taq* polymerase (Jumpstart REDtaq Ready Mix PCR Reaction Mix, Sigma, Oakville, ON, Canada) and primers specific for wildtype or knockout genes, and were detected using traditional PCR methods. Mice were used at 10 months of age. All animals were housed individually under a 12-12h light-dark cycle in a temperature controlled room (20-21°C) and were given food and water *ad libitum.* Animal usage in this study followed protocols that were approved by the York University Animal Care Committee, in accordance with the Canadian Council on Animal Care.

In vivo stimulation protocol. Portable stimulation devices were unilaterally implanted into the animals as previously described (20). In brief, rats were anesthetized with a ketamine-xylazine cocktail (0.2 mL/100 g body weight). Electrodes (Medwire, Leico Industries, New York, NY, USA) located unilaterally at either side of the common peroneal nerve caused palpable contractions in the tibialis anterior (TA) and extensor

digitorum longus (EDL) muscles. All implantations were followed by a week-long recovery period, upon which stimulation began. The CCA protocol lasted for 3 hours a day, for 7 days, with 21 hour recovery periods in between. The stimulation frequency was 10 Hz. Stimulation units were externalized for the SD rats (20), while the F344XBN rats had silicone-encased stimulators inserted into the intraperitoneal cavity, and sutured to the musculature of the abdomen (16). All other surgical procedures and stimulation protocols were identical between the two rat strains. The rats were then anesthetized and the stimulated TA and EDL muscles were removed. The non-stimulated, contralateral muscles served as internal controls. Upon removal, half of the TA muscles were used immediately for mitochondrial isolation. The remaining half of the TA, as well as the EDL muscles, were frozen in liquid nitrogen and pulverized into a fine powder for subsequent experiments. The animals were sacrificed by removal of the heart.

In vivo denervation protocol. Male, 6-month old, SD rats underwent unilateral common peroneal denervation as previously described (10). Briefly, rats were anesthetized with a ketamine-xylazine mix (0.2 ml/100 g body weight). The common peroneal nerve was exposed and a 0.5 cm long segment was removed. Following 7 days, both EDL muscles were removed and the non-denervated, contralateral muscles were used as internal controls. The tissues were then frozen in liquid nitrogen, and then pulverized into a fine powder.

Cytochrome c oxidase (COX) activity. COX activity was used as a marker of mitochondrial biogenesis. Pulverized whole muscle homogenates were prepared and sonicated for 10 s on ice at a power output of 20-30%. A buffered test solution was also

44

prepared, containing fully reduced horse heart cytochrome c (C-2506, Sigma, Oakville, ON, Canada). Using a multipipette, 250 µL of test solution were added to 20 µL of whole muscle homogenate in a 96-well plate. The enzyme activities of the homogenates were analyzed by measuring the maximal oxidation rate of cytochrome c. This was done via the absorbance change at 550 nm at 30 °C in a Synergy HT (Bio-tek Instruments, Winooski, VT, USA) microplate reader. For each sample, the COX activity measurement was calculated as an average of three trials.

In vitro RNA isolation and reverse transcription. Total RNA was isolated from frozen, whole muscle EDL powders. Tissue powder (~90 mg) was added to 1 mL of *TRIzol®* Reagent (Invitrogen, Carlsbad, CA, USA) and homogenized for 30 s at a power output of 30%. Upon 5 min of incubation at room temperature, 200 µL of chloroform was added and tissues were shaken for 15 s. Following another 3 min of room temperature incubation, samples were centrifuged at 4°C at 16 000 g for 15 min. Next, the upper aqueous phase of the sample was transferred into a new tube along with 500 µL of isopropanol, shaken for 15 s and left overnight at -20°C to precipitate. Samples were then centrifuged at 4°C at 16 000 g for 10 min. The resultant supernatant was discarded, and the pellet was washed with 700 µL of 75% ethanol. Following a centrifugation (10 min, 4°C), the supernatant was discarded and the pellet was resuspended in 100 µL of sterile water. The concentration and purity of the RNA were measured at 260 nm and 280 nm, respectively (Ultrospec 2100 Pro, Biochrom, Cambridge, UK). The quality of the RNA was determined by observing the 28S and 18S bands on a 1% formaldehyde-agarose gel. Following the manufacturer's recommendations, SuperScript® III reverse transcriptase

(Invitrogen, Carlsbad, CA, USA) was used to reverse transcribe 1.5 μg of total RNA into cDNA.

Real-time PCR. Using sequences from GenBank, primers were designed with Primer 3 v. 0.4.0 software (Massachusetts Institute of Technology, Cambridge, MA, USA) for genes of interest: CDS-1, CLS, Taz, ALCAT1, MitoPLD and Plscr3 (Tables 1-2). Primer specificity was confirmed by OligoAnalyzer 3.1 (Integrated DNA Technologies, Toronto, ON, Canada). mRNA expression was measured with SYBR® Green chemistry (PerfeCTa SYBR® Green SuperMix, ROX, Quanta BioSciences, Gaithersburg, MD, USA). Each well contained: SYBR® Green SuperMix, forward and reverse primers (20 μM), sterile water and 10 ng of cDNA. In cases where functioning primers could not be designed, 1.25 μL of TaqMan probes was used along with 12.5 μL TaqMan Universal Master Mix (4304437, Life Technologies, Carlsbad, CA, USA; Table 1) with 10 ng of cDNA and 7.25 μL of water per well. The detection of all real-time PCR amplification took place in a 96-well plate using a StepOnePlus® Real-Time PCR System (Applied Biosystems Inc., Foster City, CA, USA). The final reaction volume of each well was 25 μL. Samples were run in duplicates to ensure accuracy. The PCR program consisted of an initial holding stage (95°C for 10 min), followed by 40 amplification cycles (60°C for 1 min, 95°C for 15 s), and was completed with a final melting stage (95°C for 15 s, 60°C for 1 min, 95°C for 15 s). Nonspecific amplification and primer dimers were controlled for by the analysis of melt curves generated by the instrument for SYBR® Green analyses. Negative control wells contained water in place of cDNA.

Real-time PCR quantification. First, the threshold cycle (C_T) number of the endogenous reference gene was subtracted from the C_T number of the target gene ($\Delta C_T = C_{T(target)} - C_{T(reference)}$). Next, the ΔC_T value of the control tissue was subtracted from the ΔC_T value of the experimental tissue ($\Delta\Delta C_T = \Delta C_{T(experimental)} - \Delta C_{T(control)}$). Results were reported as fold-changes using the $\Delta\Delta C_T$ method, calculated as $2^{-\Delta\Delta C_T}$. Different endogenous control genes were tested and selected based on the highest *p*-value computed in a t-test comparing control and experimental muscles. The C_T values of selected control genes were averaged using RT^2 Profiler PCR Array Data Analysis software (http://pcrdataanalysis.sabiosciences.com /pcr/arrayanalysis.php, SABiosciences, QIAGEN Inc., Toronto, ON, Canada). For CCA, myelocytomatosis oncogene (Myc) and ribosomal protein Rps12 were chosen, while primers detecting glyceraldehyde-3-phosphate dehydrogenase (Gapdh) and β-Actin were used as endogenous controls for the denervated samples. Rps12 was used as an endogenous control for the aged CCA samples, while Rps12 and β-Actin were averaged for aged denervated samples. For PGC-1α mouse tissues, β2-microglobulin, β-Actin and Gapdh were averaged (Table 2).

Subsarcolemmal (SS) mitochondria isolation. TA muscles were excised and tissues were immediately submerged in 10-20 mL of buffer. The TA muscles were then patted dry, cut away from any excess connective tissue or fat, minced and homogenized. The mitochondrial SS isolation procedure has been previously described (9). The mitochondria were suspended in resuspension medium and were then used in flow cytometry. The amount of mitochondrial protein was determined using the Bradford protein assay.

Mitochondrial cardiolipin content. Flow cytometry was used to measure CL content in isolated SS mitochondria using a four-colour FACSCalibur flow cytometer equipped with a 488 nm argon laser (Becton Dickinson, San Jose, CA, USA). Mitochondrial CL content was measured using the fluorescent probe 10-N-Nonyl-3,6-bis(dimethylamino) acridine orange (NAO) as previously described (5). Measurements were made on taken from 50 μg of SS mitochondria isolated from rat or mouse TA muscles. Data were collected from the forward-scatter and side-scatter light detectors. The flow cytometry data were obtained following a minimum of 20 000 gated events.

Statistical Analyses. To compare between control vs. stimulated and control vs. denervated muscles, paired t-tests were performed, while wildtype vs. knockout muscles were compared using unpaired t-tests. A split-plot ANOVA calculation was used to analyze results from the CCA and denervated tissues within the aging muscles, followed by a Bonferroni *post hoc* test. To analyze the relative expression of the different transcripts, a one-way ANOVA was performed with a Bonferroni *post hoc* test. All statistical analyses were performed using GraphPad Prism 4.0 software. The critical p-value was set at $p<0.05$. All error bars represent the standard error of the mean.

Table 1. List of enzyme names, abbreviations and functions.

Enzyme Name	Abbreviation	Function
CTP:PA cytidylyltransferase	CDS-1	Rate-limiting step of CL *de novo* biosynthesis
Cardiolipin synthase	CLS	Final enzyme in CL *de novo* biosynthesis
Tafazzin	Taz	Remodels CL fatty acid to mature form
Acyl-CoA:lysocardiolipin acyltransferase-1	ALCAT1	Remodels CL fatty acid to immature form
Mitochondrial phospholipase D	MitoPLD	Cleaves CL present on outer membrane to phosphatidic acid
Phospholipid scramblase-3	Plscr3	Transfers CL to the outer membrane

Table 2. List of primer sequences and probes used in qPCR analyses. Alternative names used in this paper are written in parentheses.

Gene, Size (bp)	Type	Accession Number	Forward Primer	Reverse Primer
CDS-1	Rat	NM_031242.2	Applied Biosystems TaqMan Probe Assay ID Rn00579942_m1	
Lclat1 (ALCAT1)	Rat	XM_343020.4	Applied Biosystems TaqMan Probe Assay ID Rn01468447_m1	
Rps12	Rat	NM_031709.3	Applied Biosystems TaqMan Probe Assay ID Rn01789993_u1	
Myc	Rat	NM_012603.2	Applied Biosystems TaqMan Probe Assay ID Rn00561507_m1	
Gapdh	Rat	NM_017008.13	Applied Biosystems TaqMan Probe Assay ID Rn01775763_g1	
β-Actin	Rat	NM_031144.2	Applied Biosystems TaqMan Probe Assay ID Rn00667869_m1	
Crls1 (CLS), 66	Rat	NM_001014258.1	5'-AAT GTT GAT CGC TGC TGT GTT T-3'	5'-TTA GCT AGT GTT CGC GGT GTT G-3'
Taz, 63	Rat	NM_001025748.1	5'-CGG CTG ATT GCT GAG TGT CA-3'	5'-TCA TTC ATT CCA ACA TGC CAT AG-3'
Pld6 (MitoPLD) 116	Rat	XM_220517.3	5'-TCA TCA CGG ACT GCG ACT A-3'	5'-GGC AAA CTT ATG GTG CAT GT-3'
Plscr3, 120	Rat	NM_001012139.2	5'-GCA CCA AAG ATG GCA GAT A-3'	5'-TAA TAG CTG TAG GGT TGG GAC C-3'
Myc, 123	Rat	NM_012603.2	5'-GCT CTG CTC TCC GTC CTA TGT-3'	5'-ATG ACC GAG CTA CTT GGA GG-3'
Rps12, 127	Rat	NM_031709.3	5'-ATG GAC GTC AAC ACT GCT CT-3'	5'-ATC TCT GCG TGC TTG CAT-3'
Gapdh, 122	Rat	NM_017008.3	5'-CTC TCT GCT CCT CCC TGT TCT A-3'	5'-GGT AAC CAG GCG TCC GAT AC-3'
β-Actin, 154	Rat	NM_031144.2	5'-CCC CAT TGA ACA CGG CAT T-3'	5'-GCC AAC CGT GAA AAG ATG ACC-3'
CDS-1	Mouse	NM_173370.3	Applied Biosystems TaqMan Probe Assay ID Mm01208328_m1	
B2M	Mouse	NM_009735.3	Applied Biosystems TaqMan Probe Assay ID Mm00437762_m1	
β-Actin	Mouse	NM_007393.3	Applied Biosystems TaqMan Probe Assay ID Mm00607939_s1	
Gapdh	Mouse	NM_008084.2	Applied Biosystems TaqMan Probe Assay ID Mm99999915_g1	
Crls1, 107	Mouse	NM_001024385.1	5'-GGT GTT GCACAGCATTCA-3'	5'-GCT GGA TCT GGG TGC TTC T-3'
Taz, 205	Mouse	NM_001173547.1	5'-CCC TCC ATG TGA AGT GGC CAT TCC-3'	5'-TGG TGG TTG GAG ACG GTG ATA AGG-3'
Lclat1 (ALCAT1) 111	Mouse	NM_001081071.2	5'-AGC TGT TTG ACT CCC TAG T-3'	5'-TGA TCC ATC AGA GAA ACT TA-3'
Pld6, (MitoPLD) 127	Mouse	NM_183139.2	5'-CAC AAG TTT GCC ATC GTT GA-3'	5'-GGA ACA GCC GCA CAT ACT-3'
Plscr3, 100	Mouse	NM_023564.4	5'-CTG ATC GCC AAC CTG TTC TA-3'	5'-CTT CGC GAT TCA TCC TTA GT-3'
B2M, 106	Mouse	NM_009735.3	5'-GGT CTT TCT GGT GCT TGT CT-3'	5'-TAT GTT CGG CTT CCC ATT CT-3''
β-Actin, 117	Mouse	NM_007393.3	5'- TGT GAC GTT GAC ATC CG TAA—3''	5'- GCT AGG AGC CAG AGC AGT AA—3''
Gapdh, 113	Mouse	NM_008084.2	5'-AAC ACT GAG CAT CTC CCT CA-3''	5'-GTG GGT GCA GCG AAC TTT AT—3''

Results

Chronic muscle use. We elicited the effects of chronic muscle use by employing the chronic contractile activity (CCA) model. COX activity was used as a marker of mitochondrial content. CCA resulted in a 40% increase ($p < 0.05$) in COX activity per gram of muscle compared to the contralateral control muscles (Fig.1A). Previous work in our laboratory has shown that seven days of CCA increases CL content by 48% (20), reflecting changes in mitochondrial content, since the levels closely paralleled COX activity, as well as possible changes in organelle composition. We also measured the mRNA expression of CDS-1, CLS, Taz, ALCAT1, MitoPLD and Plscr3. With CCA, the mRNA levels of CDS-1 and Plscr3 increased significantly by 128% and 90%, respectively. In contrast, CCA led to decreases in ALCAT1 and MitoPLD mRNA levels of 32% and 40%, respectively ($p < 0.05$; Fig. 1C).

Chronic muscle disuse. To contrast with chronic muscle use, we employed denervation, a model of muscle disuse. Seven days of denervation lead to a significant 33% decrease in COX activity ($p < 0.05$; Fig. 2A). Previous work has shown that a similar period of denervation decreases CL content by 40% (22), thus matching the observed change in COX activity. Following denervation, the mRNA expression of CDS-1, CLS, ALCAT1 and Plscr3 all increased by 280%, 58%, 290% and 59%, respectively ($p < 0.05$; Fig. 2B), while the expression of Taz and MitoPLD remained unaltered.

Chronic muscle use and aging. In aged animals, muscle COX activity was diminished by 15-20%. CCA resulted in a 50% increase in COX activity in young animals, but only in a 40% augmentation in the aged animals ($p < 0.05$; Fig.3A).

51

Mitochondrial CL content was increased by 26% with CCA ($p < 0.05$), but only in young animals as this response was eliminated with age (Fig.3B). This reflects a change in organelle composition with CCA, since CL was measured in the mitochondrial fraction. With respect to CL metabolism enzymes, CDS-1 expression increased significantly by 240% in young, and by 88% in aged animals following CCA, while CLS remained unaltered ($p < 0.05$; Fig.3C-D). With respect to the CL remodelling enzymes, Taz mRNA levels were not altered by CCA, or aging. The mRNA levels of ALCAT1 and MitoPLD both decreased by 30% as a result of CCA in young animals, while Plscr3 increased by 178%. These three effects were all attenuated with age ($p < 0.05$; Figs.4B-D).

Chronic muscle disuse and aging. A separate set of aged animals was used to investigate the combined effect of aging and chronic muscle disuse produced by denervation. In these animals, a 30% difference in COX activity was observed between muscles of young and old animals. Denervation resulted in a 50% and 34% decrease in mitochondrial content in both the young and aged muscles, respectively ($p < 0.05$; Fig.5A). CDS-1 mRNA expression increased by 100% following denervation in young animals only ($p < 0.05$; Fig.5B), while CLS increased by 56% and 38% in the young and aged animals, respectively ($p < 0.05$; Fig.5C). When we measured CL remodelling enzyme expression, there was no effect of denervation or aging on Taz (Fig.6A) or MitoPLD (Fig.6C) mRNA levels. ALCAT1, however, increased with denervation by 208%. While ALCAT1 did not change with aging in control muscle, it decreased by 67% in aged, denervated muscle (Fig.6B). For Plscr3, we observed 33% and 20% increases following denervation in young and aged animals, respectively ($p < 0.05$; Fig.6D).

PGC-1α knockout conditions. To investigate a role for the transcriptional coactivator PGC-1α in the regulation of CL metabolism, we used PGC-1α knockout animals. Muscle from the animals exhibited a 42% decrease in COX activity relative to wildtype animals, reflecting a decline in organelle content per gram of muscle. CL content in the SS mitochondrial fraction remained unaltered (p<0.05; Figs.7A-B). The lack of PGC-1α resulted in a significant decrease in CDS-1 (61%) while ALCAT1 significantly increased by 97% (p<0.05; Fig.7C).

Relative gene expression levels in rats and mice. We also sought to use a comparative approach to analyze the relative mRNA expression levels of CL metabolism enzymes in rat and mouse muscle. Of the CL *de novo* biosynthesis enzymes, CDS-1 had the lowest level of expression in both the rat and mouse. This is consistent with CDS-1 as the rate-limiting enzyme in the CL synthesis pathway. Of the remodelling enzymes, the expression of Taz and ALCAT1 was similar in the rat, however, Taz was significantly higher than ALCAT1 in mouse. When we compared the expression levels of the OMM enzymes MitoPLD and Plscr3, we found Plscr3 to be significantly higher than MitoPLD in both species (Fig.8A-B; p<0.05).

Discussion

The objective of this study was to investigate the underlying basis for previously discovered findings that CL concentration increases with muscle use, and decreases with muscle disuse. To do this, we used similar conditions of muscle use and disuse as previously reported, and measured COX activity to confirm that we were successful at altering mitochondrial content. We next set out to compare the CL content in muscle under these conditions, with the expression of the enzymes involved in the CL metabolism pathway. We chose to examine the mRNA levels of these enzymes 1) due to the lack of suitable antibodies and 2) to provide a comprehensive analysis of the trends in gene expression within the pathway as produced by stimuli which alter mitochondrial biogenesis.

We analyzed enzymes of the CL *de novo* biosynthesis, remodelling and outer mitochondrial membrane pathways following CCA, denervation, and another from of muscle disuse, aging. Our expectation was that the expression of the biosynthesis enzymes CDS-1 and CLS would increase with CCA and decrease with denervation, thus paralleling mitochondrial and CL content. We found that CCA induced an increase in CDS-1, while CLS remained unaltered. Thus, the increase in CL content measured with muscle use is accompanied by the up-regulation of certain, but not all CL biosynthesis genes. Since CDS-1 is the rate-limiting enzyme in CL biosynthesis (13), the augmented expression of CDS-1 correlates well with the increase of CL in CCA-treated muscle. Our comparative approach to analyze the relative mRNA levels of these enzymes confirmed the probable rate-limiting function of CDS-1, since CDS-1 mRNA levels were among the

lowest of the genes measured in both rat and mouse muscle. However, we were surprised to find that denervation also elicited increases in the mRNAs encoding these biosynthesis enzymes. Our observations are suggestive of a secondary, compensatory response which occurs during chronic muscle disuse to restore the lost organelle CL content during this condition (22).

Taz and ALCAT1 are enzymes responsible for the remodelling of CL FAs. Taz has been shown to transfer linoleic FAs onto CL, thus creating mature, functional tetralinoleic CL. A loss of function mutation in the Taz gene in humans has been shown to lead to Barth syndrome, which is characterized by numerous myopathies (3). In contrast, ALCAT1 has been shown to add polyunsaturated FAs onto CL, creating an immature form of the molecule which is elevated during pathological conditions (14). Based on this, we hypothesized that Taz and ALCAT1 expression would change in opposite directions with chronic muscle use, and also with muscle disuse conditions. Surprisingly, Taz was completely unresponsive to the treatments. However, ALCAT1 decreased with CCA, and became elevated following denervation. This suggests that chronic muscle use not only elevates CL levels, but also serves to induce a more functional form of the phospholipid. Interestingly, the higher level of Taz relative to ALCAT1 in the mouse, compared to the rat, suggests that CL in mouse muscle may have a greater ratio of functional to nonfunctional CL than in rat muscle.

MitoPLD and Plscr3 both interact with CL on the outer mitochondrial membrane. Plscr3 serves to transport CL from the inner to the outer mitochondrial membrane, thereby dispersing CL within the organelle. MitoPLD, on the other hand, cleaves outer

membrane CL into PA, thereby reducing total CL content. We hypothesized that CCA would induce Plscr3 to help redistribute the increase in CL content, while MitoPLD would decline to facilitate this process. We found that CCA elicited this response in both of these enzymes, supporting our hypothesis. To our surprise, denervation elicited a similar effect. We speculate that this alteration may serve a very different purpose during chronic muscle disuse. The increase in outer mitochondrial membrane CL may act as a binding site for tBid, which triggers cytochrome c release and leads to mitochondrially-mediated apoptosis. Thus, the effect may be a contributing factor to the previously reported increased apoptotic susceptibility following denervation (1). Our comparative analyses of mRNA levels showed the existence of high ratios of Plscr3 relative to MitoPLD in both mouse and rat. This suggests that the need for CL transport to the outer membrane is greater than that for CL cleavage under steady state conditions.

When we analyzed the CL levels within mitochondria of young and aged animals, we found no difference between the two age groups. This finding was in parallel with the lack of difference exhibited for the measured mRNAs. In general, the response of aging animals to either CCA or denervation was attenuated compared to the responses observed in young animals. Notably, both the protective CCA-, and the detrimental denervation-induced changes of ALCAT1 were lost with age. CCA-induced changes of MitoPLD and Plscr3 were also both reduced with aging. These findings are consistent with the observation that aging muscle can adapt to variations in chronic muscle use or disuse, but that the response is attenuated compared to that in young muscle (17).

In an effort to elucidate the transcriptional underpinnings behind our observations, we examined the possible role of PGC-1α. PGC-1α is an established nuclear coactivator, often referred to as the master regulator of mitochondrial biogenesis because its activation or overexpression promotes the transcription of a wide variety of nuclear gene products that are destined for the mitochondria. However, its function is currently unknown regarding its regulation of the transcripts of genes encoding enzymes of CL. PGC-1α has been shown to be elevated by CCA (2), while chronic muscle disuse via denervation downregulates PGC-1α levels (1). Thus, we used PGC-1α knockout animals to determine whether this transcriptional coactivator is involved in mediating the mRNA changes observed. We found that CDS-1 was suppressed by the absence of PGC-1α, suggesting that the coactivator directly regulates CL expression of this rate-limiting enzyme, and therefore the flux through the CL biosynthesis pathway. Indeed, inspection of the CDS-1 promoter reveals binding sites for MyoD, USF-1, NF-kappa B, PPAR-gamma, CREB and MEF-2, all transcription factors through which PGC-1α may be acting. Considerable further work is required to verify the possible functional nature of these binding sites within the CDS-1 promoter region. With respect to the remodelling enzymes, ALCAT1 levels were increased in the absence of PGC-1α. This suggests that PGC-1α normally suppresses ALCAT1, thereby exhibiting a protective role on the fatty acid composition of CL. In contrast, neither of the outer membrane CL remodelling genes was affected by the absence of PGC-1α. Thus, PGC-1α has a selective role in regulating the transcription of CL metabolism enzymes.

This study provides the first detailed analysis of the expression of CL synthesis and remodelling enzymes in skeletal muscle. Our results set the stage for further exploration of this complex network of mitochondrial membrane regulators, particularly when suitable antibodies become available. Both protein level measurements, as well as the localization of these enzymes will be crucial for the expansion of our knowledge regarding this molecular pathway. All CL biosynthetic enzymes are nuclear-encoded proteins. Thus, they rely on the mitochondrial import machinery in order to be transported into the mitochondria to manufacture or modify CL. It would therefore be of great interest to analyze the trafficking, localization and possible post-translational modifications of many of these enzymes following chronic muscle use or disuse, or in diseases of phospholipid metabolism. Our data suggest that the transcriptional activation of certain genes responsible for CL synthesis is upregulated during muscle use, perhaps to produce more CL, and also during muscle disuse as part of a possible compensatory mechanism. Many of these observed effects are lost with aging. Finally, it was notable that some CL metabolism genes are regulated by PGC-1α, documenting a role for this coactivator in mitochondrial phospholipid synthesis, alongside its well established function in the regulation of typical nuclear genes encoding mitochondrial proteins.

Acknowledgements

Reference List

1. **Adhihetty PJ, O'Leary MF, Chabi B, Wicks KL and Hood DA.** Effect of denervation on mitochondrially mediated apoptosis in skeletal muscle. *J Appl Physiol* 102: 1143-1151, 2007.

2. **Baar K, Wende AR, Jones TE, Marison M, Nolte LA, Chen M, Kelly DP and Holloszy JO.** Adaptations of skeletal muscle to exercise: rapid increase in the transcriptional coactivator PGC-1. *FASEB J* 16: 1879-1886, 2002.

3. **Barth PG, Scholte HR, Berden JA, Van der Klei-Van Moorsel JM, Luyt-Houwen IE, Van 't Veer-Korthof ET, Van der Harten JJ and Sobotka-Plojhar MA.** An X-linked mitochondrial disease affecting cardiac muscle, skeletal muscle and neutrophil leucocytes. *J Neurol Sci* 62: 327-355, 1983.

4. **Bione S, D'Adamo P, Maestrini E, Gedeon AK, Bolhuis PA and Toniolo D.** A novel X-linked gene, G4.5. is responsible for Barth syndrome. *Nat Genet* 12: 385-389, 1996.

5. **Chabi B, Ljubicic V, Menzies KJ, Huang JH, Saleem A and Hood DA.** Mitochondrial function and apoptotic susceptibility in aging skeletal muscle. *Aging Cell* 7: 2-12, 2008.

6. **Chen D, Zhang XY and Shi Y.** Identification and functional characterization of hCLS1, a human cardiolipin synthase localized in mitochondria. *Biochem J* 398: 169-176, 2006.

7. **Chicco AJ and Sparagna GC.** Role of cardiolipin alterations in mitochondrial dysfunction and disease. *Am J Physiol Cell Physiol* 292: C33-C44, 2007.

8. **Choi SY, Huang P, Jenkins GM, Chan DC, Schiller J and Frohman MA.** A common lipid links Mfn-mediated mitochondrial fusion and SNARE-regulated exocytosis. *Nat Cell Biol* 8: 1255-1262, 2006.

9. **Cogswell AM, Stevens RJ and Hood DA**. Properties of skeletal muscle mitochondria isolated from subsarcolemmal and intermyofibrillar regions. *Am J Physiol* 264: C383-C389, 1993.

10. **Eisenberg HA and Hood DA**. Blood flow, mitochondria, and performance in skeletal muscle after denervation and reinnervation. *J Appl Physiol* 76: 859-866, 1994.

11. **Gebert N, Joshi AS, Kutik S, Becker T, McKenzie M, Guan XL, Mooga VP, Stroud DA, Kulkarni G, Wenk MR, Rehling P, Meisinger C, Ryan MT, Wiedemann N, Greenberg ML and Pfanner N**. Mitochondrial cardiolipin involved in outer-membrane protein biogenesis: implications for Barth syndrome. *Curr Biol* 19: 2133-2139, 2009.

12. **Gonzalvez F, Pariselli F, Dupaigne P, Budihardjo I, Lutter M, Antonsson B, Diolez P, Manon S, Martinou JC, Goubern M, Wang X, Bernard S and Petit PX**. tBid interaction with cardiolipin primarily orchestrates mitochondrial dysfunctions and subsequently activates Bax and Bak. *Cell Death Differ* 12: 614-626, 2005.

13. **Hatch GM**. Cardiolipin biosynthesis in the isolated heart. *Biochem J* 297 (Pt 1): 201-208, 1994.

14. **Li J, Romestaing C, Han X, Li Y, Hao X, Wu Y, Sun C, Liu X, Jefferson LS, Xiong J, Lanoue KF, Chang Z, Lynch CJ, Wang H and Shi Y**. Cardiolipin remodeling by ALCAT1 links oxidative stress and mitochondrial dysfunction to obesity. *Cell Metab* 12: 154-165, 2010.

15. **Lin J, Wu PH, Tarr PT, Lindenberg KS, St-Pierre J, Zhang CY, Mootha VK, Jager S, Vianna CR, Reznick RM, Cui L, Manieri M, Donovan MX, Wu Z, Cooper MP, Fan MC, Rohas LM, Zavacki AM, Cinti S, Shulman GI, Lowell BB, Krainc D and Spiegelman BM**. Defects in adaptive energy metabolism with CNS-linked hyperactivity in PGC-1alpha null mice. *Cell* 119: 121-135, 2004.

16. **Ljubicic V and Hood DA**. Diminished contraction-induced intracellular signaling towards mitochondrial biogenesis in aged skeletal muscle. *Aging Cell* 8: 394-404, 2009.

17. **Ljubicic V, Joseph AM, Adhihetty PJ, Huang JH, Saleem A, Uguccioni G and Hood DA.** Molecular basis for an attenuated mitochondrial adaptive plasticity in aged skeletal muscle. *Aging (Albany NY)* 1: 818-830, 2009.

18. **Schlame M, Rua D and Greenberg ML.** The biosynthesis and functional role of cardiolipin. *Prog Lipid Res* 39: 257-288, 2000.

19. **Sen T, Sen N, Tripathi G, Chatterjee U and Chakrabarti S.** Lipid peroxidation associated cardiolipin loss and membrane depolarization in rat brain mitochondria. *Neurochem Int* 49: 20-27, 2006.

20. **Takahashi M and Hood DA.** Chronic stimulation-induced changes in mitochondria and performance in rat skeletal muscle. *J Appl Physiol* 74: 934-941, 1993.

21. **Van Q, Liu J, Lu B, Feingold KR, Shi Y, Lee RM and Hatch GM.** Phospholipid scramblase-3 regulates cardiolipin de novo biosynthesis and its resynthesis in growing HeLa cells. *Biochem J* 401: 103-109, 2007.

22. **Wicks KL and Hood DA.** Mitochondrial adaptations in denervated muscle: relationship to muscle performance. *Am J Physiol* 260: C841-C850, 1991.

Figure Legend

Figure 1. *Effects of CCA on mitochondrial content, CL levels and mRNA expression in skeletal muscle.* **(A)** Average COX activity in CCA and control muscles (n=8); **(B)** Tissue CL content in control and 7-day CCA muscles (data from Takahashi & Hood, 1993; n=7); **(C)** mRNA levels of CDS-1, CLS, Taz, ALCAT1, MitoPLD and Plscr3 in chronically stimulated muscles (n=8). Graph represents fold-changes relative to control muscles. Values are representative of means+/-SEM; p<0.05; * vs. control.

Figure 2. *Effects of denervation on mitochondrial content, CL levels and mRNA expression in skeletal muscle.* **(A)** Average COX activity in denervated and control muscles (n=8); **(B)** Tissue CL content in control and 8-day denervated muscles (data from Wicks & Hood, 1991; n=7); **(C)** mRNA levels of CDS-1, CLS, Taz, ALCAT1, MitoPLD and Plscr3 in denervated muscles (n=8). Graph represents fold-changes relative to control muscles. Values are representative of means+/-SEM; p<0.05; * vs. control.

Figure 3. *Effects of CCA and age on mitochondrial content, mitochondrial CL levels and mRNA expression in skeletal muscle.* **(A)** Average COX activity in young and aged, control and CCA muscles (n=10); **(B)** CL content of isolated SS mitochondria from young and aged, control and CCA muscles (n=9). mRNA levels of cardiolipin *de novo* biosynthesis enzymes **(C)** CDS-1; and **(D)** CLS in control and stimulated muscles of 6-month and 36-month old rats (n=6 for each group). Empty bars represent control muscles, filled bars represent CCA muscles. Values are representative of means+/-SEM; p<0.05; * vs. control; ** main effect of aging.

Figure 4. *mRNA levels of cardiolipin remodelling and outer membrane enzymes.* **(A)** Taz; **(B)** ALCAT1; **(C)** MitoPLD; and **(D)** Plscr3 in control and stimulated muscles of 6-month and 36-month old rats. Empty bars represent control muscles, filled bars represent CCA muscles. Values are representative of means+/-SEM; n=6 for each group; p<0.05; * vs. control; ** main effect of aging.

Figure 5. *Effects of denervation and age on mitochondrial content and mRNA expression in skeletal muscle.* **(A)** Average COX activity in young and aged, control and denervated muscles (n=8). mRNA levels of cardiolipin *de novo* biosynthesis enzymes **(B)** CDS-1; and **(C)** CLS in control and denervated muscles of 6-month and 36-month old rats (n=6 for each group). Empty bars represent control muscles, filled bars represent denervated muscles. Values are representative of means+/-SEM; p<0.05; * vs. control; ** main effect of aging.

Figure 6. *mRNA levels of cardiolipin remodelling and outer membrane enzymes.* **(A)** Taz; **(B)** ALCAT1; **(C)** MitoPLD; and **(D)** Plscr3 in control and denervated 6-month and 36-month old rats. Empty bars represent control muscles, filled bars represent denervated muscles. Values are representative of means+/-SEM; n=6 for each group; p<0.05; * vs. control; ** main effect of aging.

Figure 7. *Effects of PGC-1α knockout on mitochondrial content, mitochondrial CL levels and mRNA expression in skeletal muscle.* **(A)** Average COX activity of PGC-1α knockout and wildtype mice (n=4); **(B)** CL content in isolated SS mitochondria of wildtype and PGC-1α knockout muscles (n=6); **(C)** mRNA levels of CDS-1, CLS, Taz, ALCAT1, MitoPLD and Plscr3 in muscles of wildtype and PGC-1α knockout mice (n=7). Graph

represents fold-changes relative to wildtype mice. Values are representative of means+/-SEM; p<0.05; * vs. control or wildtype.

Figure 8. *Relative mRNA levels of CL metabolisms enzymes.* CL synthesis enzymes CDS-1 and CLS; CL remodelling enzymes Taz and ALCAT1; and OMM CL proteins MitoPLD and Plscr3 in **(A)** young rats (n=12); and **(B)** wildtype mice (n=7); * vs. CDS-1, p<0.05; p<0.05; □ vs ALCAT1, p<0.05; # vs MitoPLD, p<0.05. Values are representative of means+/-SEM.

Fig. 1

Fig. 2

Fig. 3

Fig. 4

A

B

C

D
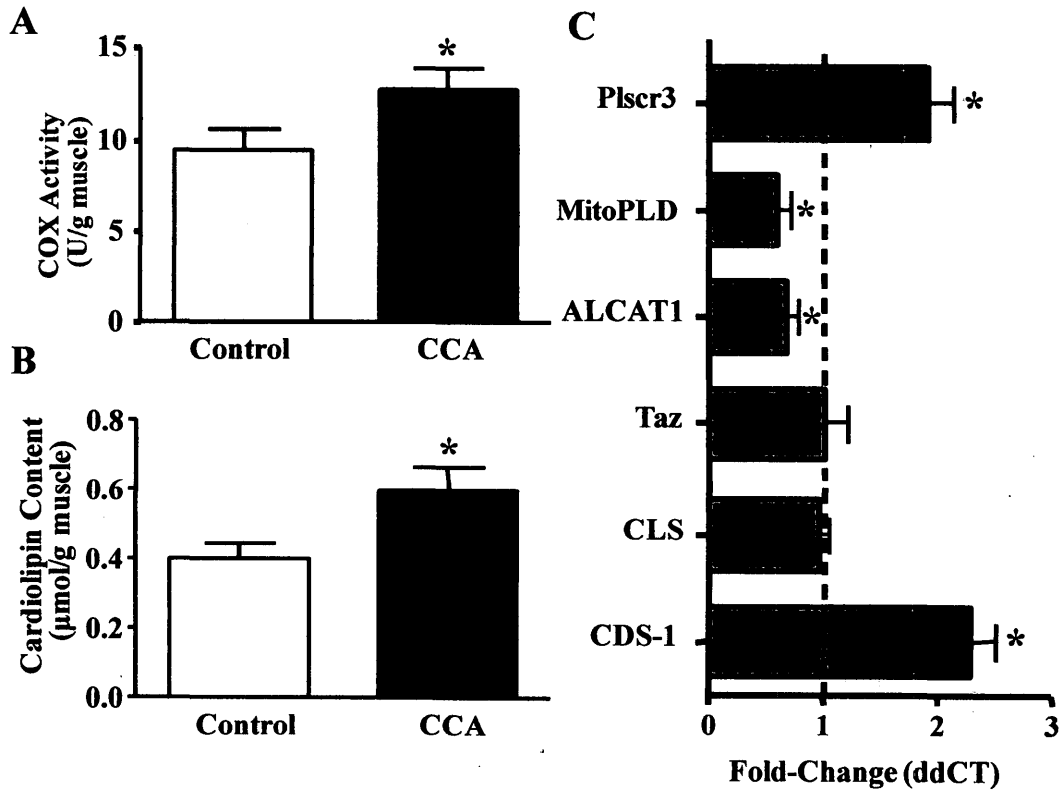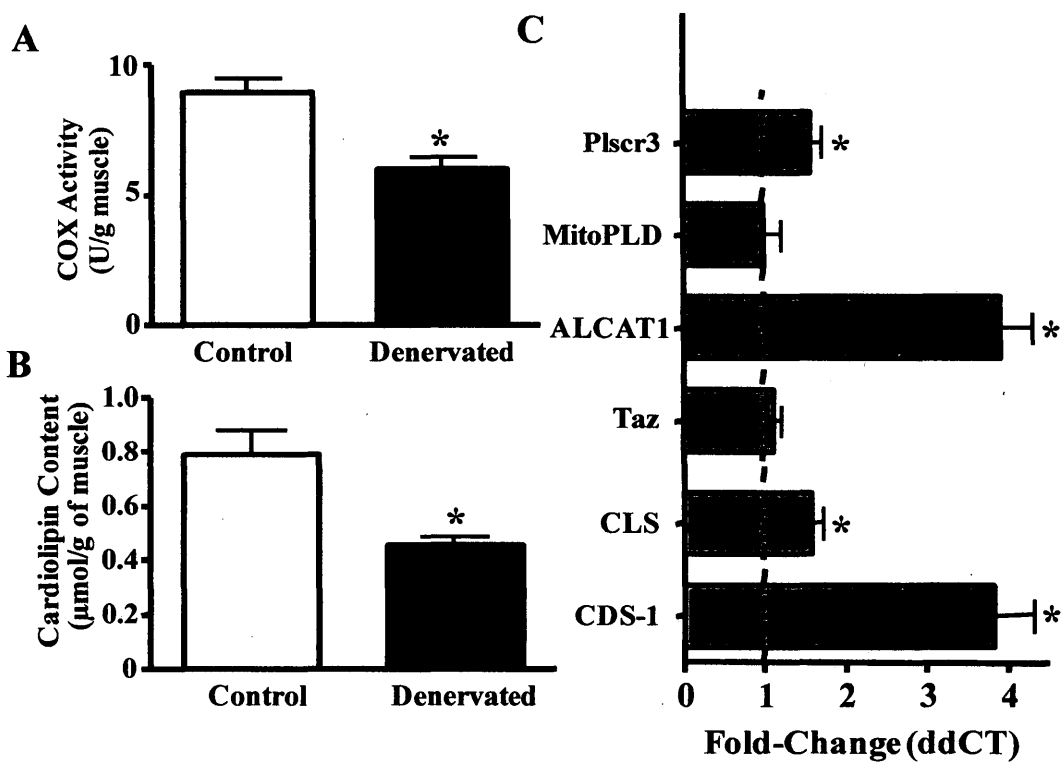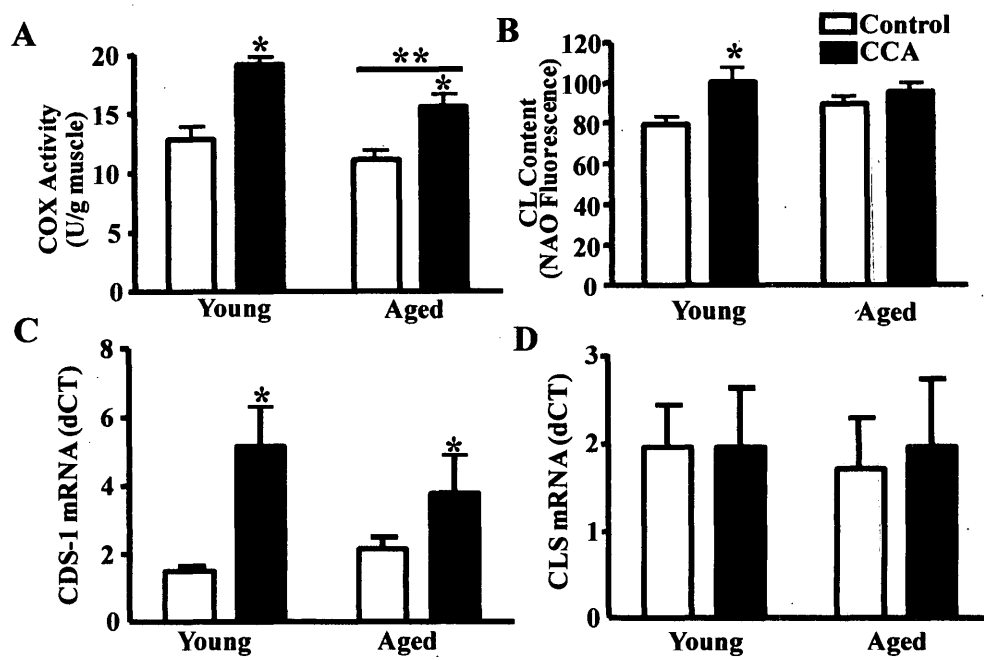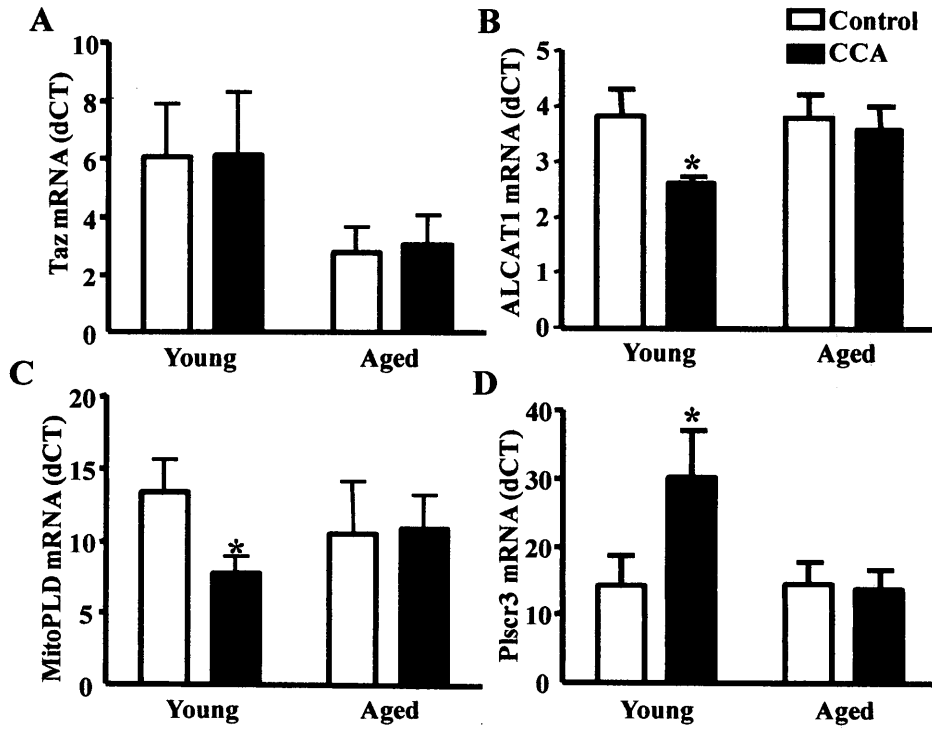
Fig. 5
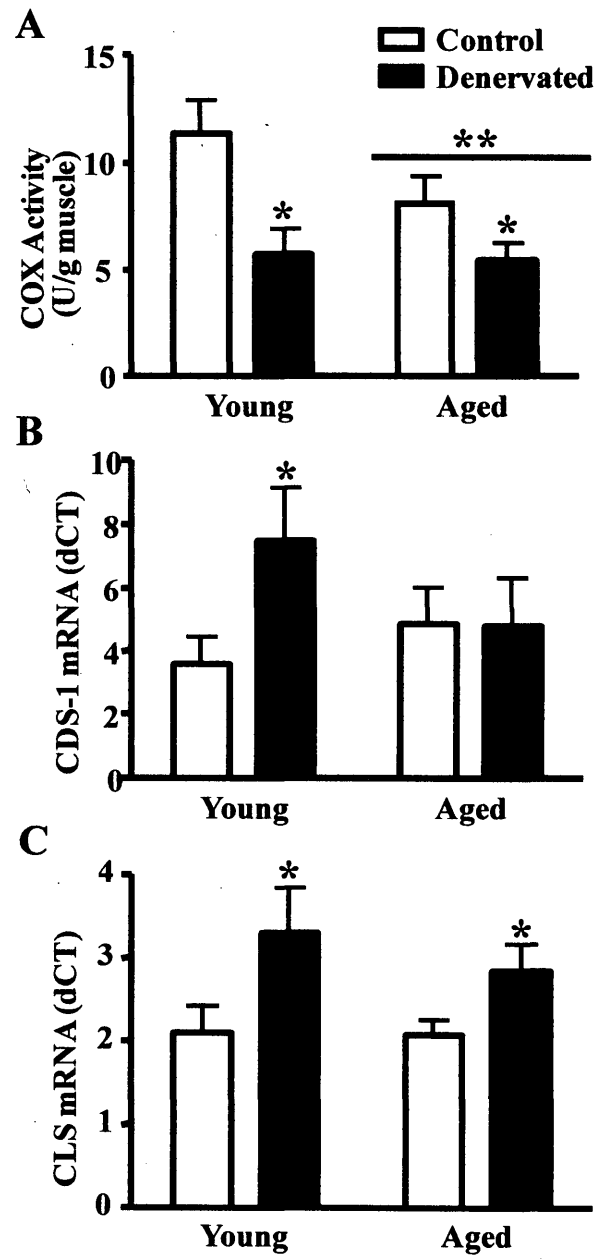
Fig. 6
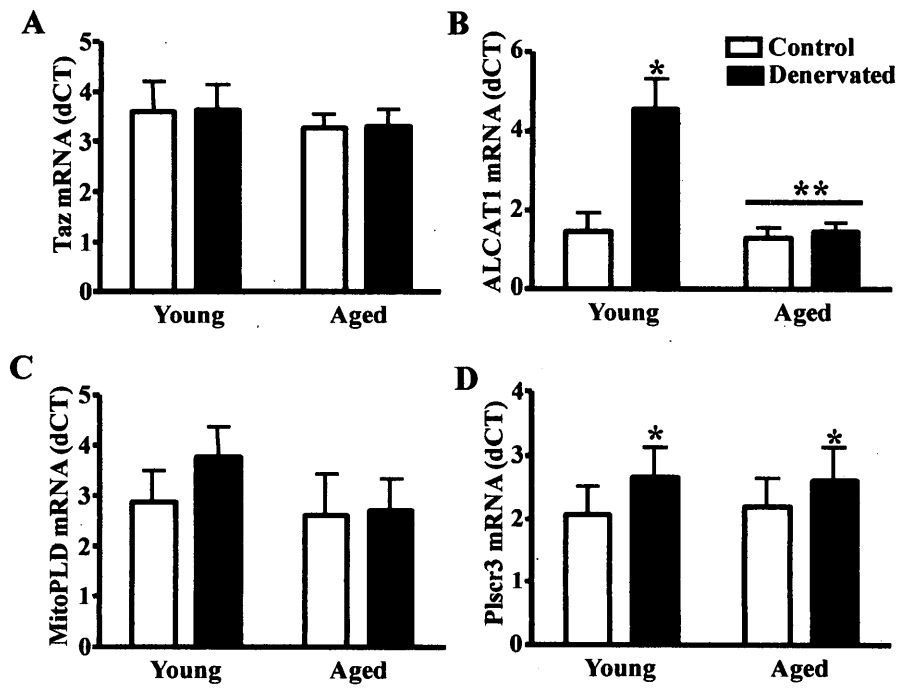
Fig. 7
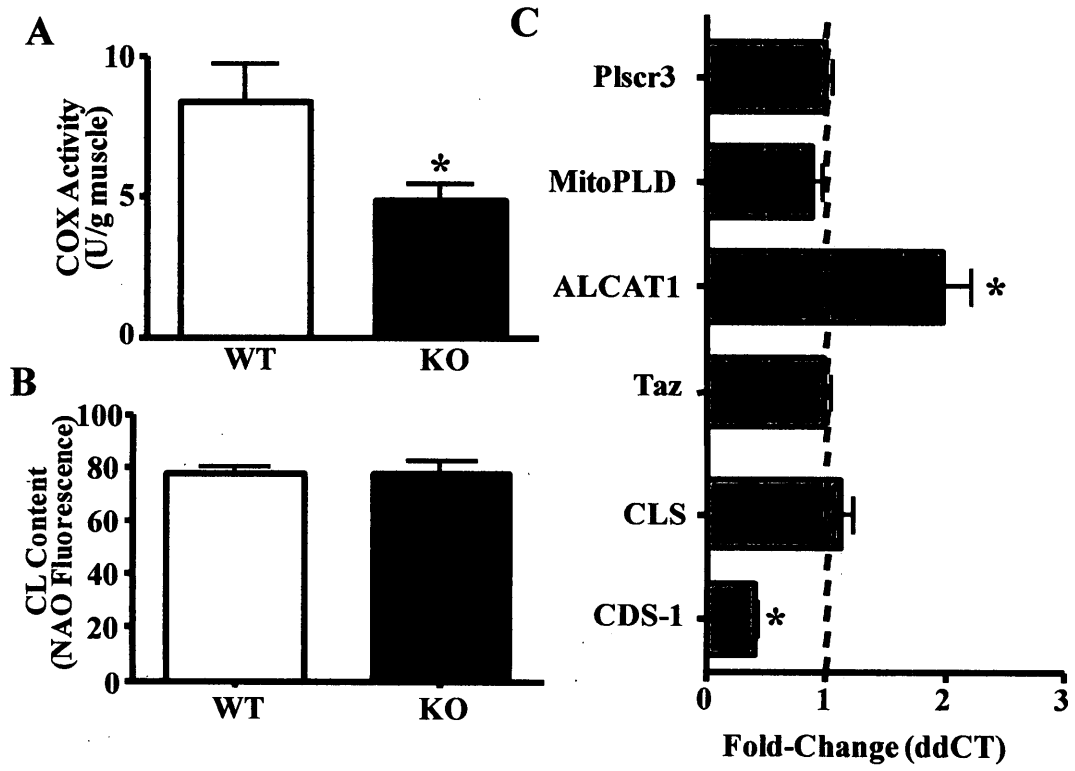
Fig. 8
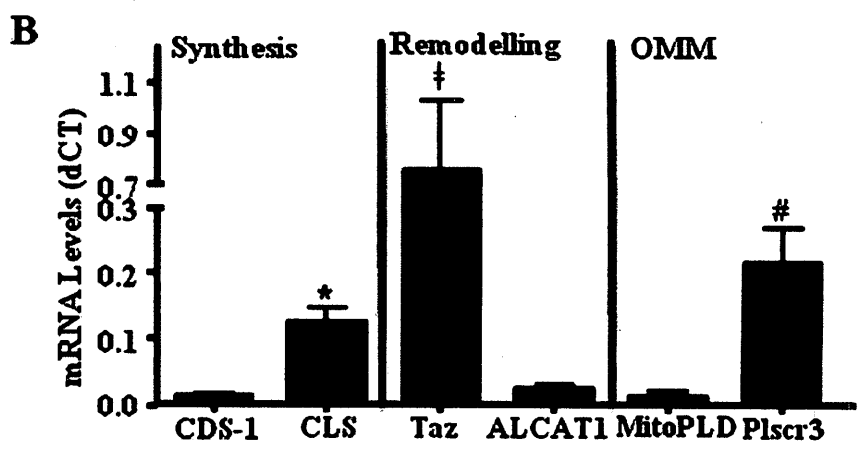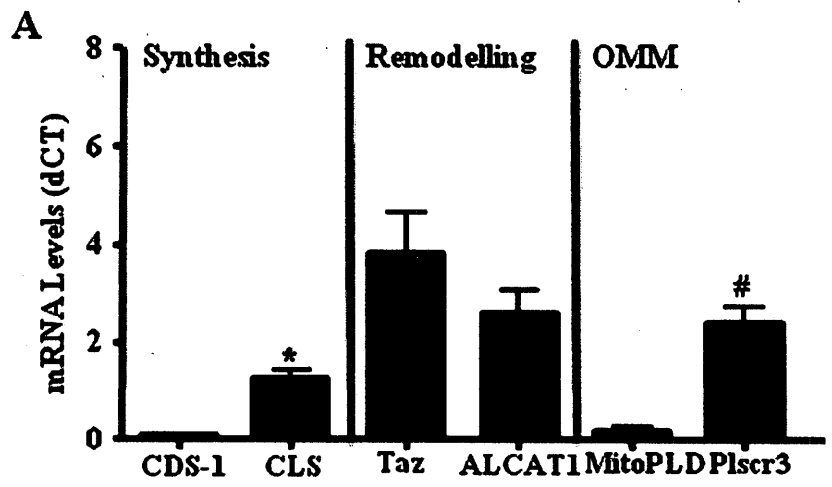
Future Work

1) We found that the conditions we placed upon the observed skeletal muscles to result in altered CL content. It would also be of interest to explore the peroxidation levels within these tissues, by isolating CL and utilizing a lipid peroxidation measurement, such as the TBARs assay.

2) Our data revealed that the transcriptional coactivator PGC-1α is involved in the regulation of two CL metabolism transcripts: CDS-1 and ALCAT1. Alas, we are unable to comment through which transcriptional machinery the coactivator is acting, based on our current results. To explore this, we will measure the effect of PGC1-α-mediated transcriptional alteration of CDS-1 or ALCAT1 promoter activity on different truncations of their respective promoters.

3) The generation of ALCAT1 knockout mice has piqued our interest regarding future work. More specifically, measuring the levels of other CL remodelling genes in the absence of ALCAT1 will shed light on whether these genes regulate the expression of one another. It would also be intriguing to examine whether any improvements in exercise performance occur, without the presence of the pathological CL remodeller.

4) Analyses of Taz knockout mice have uncovered similar maladies as those in Barth Syndrome patients, such as malfunctioning mitochondria within cardiac and skeletal muscles. It would be of interest to explore whether chronic muscle use is able to rescue the functional deficits within skeletal muscle lacking Taz.

Appendix A

Data and Statistical Analyses

Table 1A: COX Activity following 7 days of CCA

Cytochrome c Oxidase activity (U/g muscle)		
n	7 day control	7 day CCA
1	5.83	9.82
2	6.71	8.49
3	7.87	12.24
4	10.49	14.34
5	9.27	13.89
6	11.43	13.64
7	15.86	18.94
8	8.45	11.00
X ± SE	9.49 ± 1.12	12.79 ± 1.14

Paired t test
Control vs. 7 day CCA
Two-tailed P value < 0.0001
t = 8.87
df = 7

Table 1B: COX Activity following 7 days of denervation

Cytochrome c Oxidase activity (U/g muscle)		
n	7 day control	7 day denervated
1	7.37	6.15
2	8.95	6.87
3	8.26	5.18
4	11.26	8.44
5	7.84	5.34
6	9.83	5.36
7	10.76	6.02
8	7.45	4.21
X ± SE	8.97 ± 0.53	5.95 ± 0.45

Paired t test
Control vs. 7 day denervated
Two-tailed P value = 0.0002
t = 7.31
df = 7

Table 1C: COX Activity of PGC-1α Knockout mice

Cytochrome c Oxidase activity (U/g muscle)		
n	Wildtype	Knockout
1	11.08	4.91
2	8.61	5.17
3	4.86	3.14
4	9.04	6.95
X ± SE	8.40 ± 1.30	5.04 ± 0.78

Unpaired t test
Wildtype vs. Knockout
Two-tailed P value = 0.04
t = 3.325
df = 3

Table 1D: COX Activity following 7 days of denervation in young and aged animals.

n	Cytochrome c Oxidase activity (U/g muscle)			
	Young Control	Young CCA	Aged Control	Aged CCA
1	12.00	18.04	10.75	13.41
2	9.20	17.70	13.48	19.36
3	16.55	18.04	12.01	16.14
4	19.37	21.69	12.41	18.77
5	9.69	22.70	13.69	20.24
6	14.39	18.77	12.86	16.44
7	10.37	19.17	9.31	15.15
8	11.06	18.84	8.13	12.46
9	12.83	19.37	11.56	13.68
10	13.33	18.26	7.26	10.96
$X \pm SE$	9.49 ± 1.12	12.79 ± 1.14	1.38 ± 0.06	1.38 ± 0.07

Two-Way ANOVA- Young vs. Aged		
Source of Variation	P value summary	Significant?
Interaction	ns	No
Age	*	Yes
Stimulation	***	Yes

Bonferroni posttests- Young vs. Aged				
Age	Difference	t	P value	Summary
Young	6.379	7.656	P<0.001	***
Aged	4.515	5.419	P<0.001	***

Table 2A: Cardiolipin content following 7 days of CCA

n	Cardiolipin Content (μmol/g muscle)			Paired t test
	7 day control	7 day CCA		
1	0.4188	0.6792		
2	0.492	0.5248		
3	0.428	0.426		
4	0.223	0.697		Paired t test
5	0.259	0.416		Control vs. 7 day CCA
6	0.502	0.469		Two-tailed P value = 0.053
7	0.4898	0.942		t = 2.405
X ± SE	0.39 ± 0.06	0.58 ± 0.06		df = 6

Table 2B: Cardiolipin content following 7 days of denervation

n	Cardiolipin Content (μmol/g muscle)			Paired t test
	8 day control	8 day denervated		
1	1.05	0.55		
2	0.56	0.4		
3	0.73	0.35		
4	0.53	0.45		Paired t test
5	0.84	0.51		Control vs. 8 day denervated
6	1.14	0.43		Two-tailed P value = 0.0079
7	0.66	0.51		t = 3.907
X ± SE	0.79 ± 0.11	0.46 ± 0.03		df = 6

Table 2C: Cardiolipin content of PGC-1α knockout mice

n	Cardiolipin Content (NAO Fluorescence)			Unpaired t test
	PGC-1α Wildtype	PGC-1α Knockout		
1	78.82	76.19		
2	72.05	71.8		
3	78.69	89.68		Unpaired t test
4	80.83	72.85		Wildtype vs. Knockout
5	58.43	61.44		Two-tailed P value = 0.6607
6	41.41	59.36		t = 0.4522
X ± SE	68.37 ± 7.78	71.89 ± 5.49		df = 10

78

Table 3: mRNA expression of CL metabolism enzymes following CCA

CDS-1 mRNA expression (dCT)		
n	7 day control	7 day CCA
1	1.11	1.59
2	0.66	2.25
3	1.04	2.75
4	1.01	2.46
5	1.80	4.91
6	0.54	1.23
7	0.69	1.12
8	0.41	0.70
X ± SE	0.91 ± 0.15	2.13 ± 0.47

Paired t test
Control vs. 7 day CCA
Two-tailed P value = 0.0083
t = 3.638
df = 7

CLS mRNA expression (dCT)		
n	7 day control	7 day CCA
1	10.24	11.07
2	9.03	9.06
3	12.76	7.92
4	22.34	23.12
5	52.86	49.69
6	19.44	21.40
7	25.80	13.21
8	11.30	15.48
X ± SE	20.47 ± 5.11	18.87 ± 4.81

Paired t test
Control vs. 7 day CCA
Two-tailed P value = 0.42
t = 0.86
df = 7

Taz mRNA expression (dCT)		
n	7 day control	7 day CCA
1	77.43	35.30
2	37.71	31.21
3	70.81	24.46
4	91.50	70.14
5	213.92	105.49
6	76.19	139.97
7	59.61	105.50
8	10.86	16.79
X ± SE	79.75 ± 21.19	66.10 ± 16.31

Paired t test
Control vs. 7 day CCA
Two-tailed P value = 0.50
t = 0.71
df = 7

ALCAT1 mRNA expression (dCT)		
n	7 day control	7 day CCA
1	5.00	6.48
2	7.66	3.49
3	9.50	6.26
4	5.92	5.26
5	6.87	1.33
6	5.71	6.24
7	4.77	3.43
8	11.48	5.55
X ± SE	7.11 ± 0.82	4.76 ± 0.64

			Paired t test
			Control vs. 7 day CCA
			Two-tailed P value = 0.0472
			t = 2.403
			df = 7

MitoPLD mRNA expression (dCT)		
n	7 day control	7 day CCA
1	1.32	0.87
2	4.28	2.55
3	0.83	1.04
4	11.97	3.49
5		
6	3.87	1.13
7	2.74	1.26
8	14.49	9.79
X ± SE	5.64 ± 1.90	2.87 ± 1.13

			Paired t test
			Control vs. 7 day CCA
			Two-tailed P value = 0.049
			t = 2.46
			df = 6

Plscr3 mRNA expression (dCT)		
n	7 day control	7 day CCA
1	148.30	165.12
2	31.95	78.39
3	77.31	221.78
4	112.45	195.13
5	170.24	275.00
6	121.15	136.28
7	89.96	243.90
8	52.38	88.40
X ± SE	100.5 ± 16.6	175.5 ± 25.27

			Paired t test
			Control vs. 7 day CCA
			Two-tailed P value = 0.006
			t = 3.85
			df = 7

Table 4: mRNA expression of CL metabolism enzymes following denervation

CDS-1 mRNA expression (dCT)		
n	7 day control	7 day denervated
1	0.004	0.008
2	0.005	0.016
3	0.003	0.015
4		
5	0.002	0.010
6	0.003	0.014
7	0.005	0.013
8	0.004	0.015
X ± SE	0.004±0.0003	0.01±0.001

Paired t test
Control vs. 7 day denervated
Two-tailed P value = 0.0002
t = 8.329
df = 6

CLS mRNA expression (dCT)		
n	7 day control	7 day denervated
1	1.60	2.58
2	1.18	1.13
3	0.45	1.05
4	0.60	0.87
5	0.35	0.62
6	0.88	1.98
7		
8	3.83	6.47
X ± SE	1.27 ± 0.43	2.10 ± 0.72

Paired t test
Control vs. 7 day denervated
Two-tailed P value = 0.049
t = 2.449
df = 6

Taz mRNA expression (dCT)		
n	7 day control	7 day denervated
1	6.70	6.14
2	3.94	3.13
3	2.33	2.08
4	1.20	1.33
5	0.95	1.16
6	2.31	4.33
7	6.38	6.64
8	12.92	14.25
X ± SE	4.59 ± 1.41	4.88 ± 1.52

Paired t test
Control vs. 7 day denervated
Two-tailed P value = 0.42
t = 0.86
df = 7

ALCAT1 mRNA expression (dCT)		
n	7 day control	7 day denervated
1	9.37	49.24
2	32.44	83.99
3	3.77	14.12
4	4.13	15.13
5	25.09	52.26
6	4.19	15.40
7	10.49	49.06
8	15.03	82.92
X ± SE	13.06±3.75	45.27±10.15

	Paired t test
	Control vs. 7 day denervated
	Two-tailed P value = 0.0036
	t = 4.3
	df = 7

MitoPLD mRNA expression (dCT)		
n	7 day control	7 day denervated
1	0.15	0.06
2	0.06	0.07
3	0.02	0.03
4	0.02	0.01
5	0.00	0.02
6	0.04	0.12
7	0.58	0.12
8	0.27	0.27
X ± SE	0.14 ± 0.07	0.08 ± 0.03

	Paired t test
	Control vs. 7 day denervated
	Two-tailed P value = 0.39
	t = 0.91
	df = 7

Plscr3 mRNA expression (dCT)		
n	7 day control	7 day denervated
1	7.37	6.15
2	8.95	6.87
3	8.26	5.18
4	11.26	8.44
5	7.84	5.34
6	9.83	5.36
7	10.76	6.02
8	7.45	4.21
X ± SE	8.97 ± 0.53	5.95 ± 0.45

	Paired t test
	Control vs. 7 day denervated
	Two-tailed P value = 0.046
	t = 2.42
	df = 7

Table 5: mRNA expression of CL metabolism enzymes following CCA and aging

n	CDS-1 mRNA expression (dCT)			
	Young Control	Young CCA	Aged Control	Aged CCA
1	0.007	0.030	0.006	0.022
2	0.004	0.011	0.009	0.011
3	0.006	0.026	0.012	0.011
4	0.004	0.010	0.003	0.002
5	0.005	0.006	0.006	0.008
6	0.004	0.019	0.007	0.024
X±SE	0.005±0.0005	0.01±0.004	0.007±0.001	0.01±0.003

Two-Way ANOVA- Young vs. Aged		
Source of Variation	P value	Significant?
Interaction	ns	No
Age	ns	No
Stimulation	**	Yes

Bonferroni posttests- Young vs. Aged				
Age	Difference	t	P value	Summary
Young	0.01208	3.502	P < 0.05	*
Aged	0.005804	1.683	P > 0.05	ns

n	CLS mRNA expression (dCT)			
	Young Control	Young CCA	Aged Control	Aged CCA
1	4.09	2.62	3.67	5.52
2	1.47	1.37	0.88	0.93
3	1.27	0.94	1.03	0.85
4	1.30	1.14	0.58	0.90
5	2.57	5.02	3.32	2.73
6	1.05	0.72	0.82	0.82
X±SE	1.96±0.48	1.97±0.67	1.72±0.57	1.96±0.77

Two-Way ANOVA- Young vs. Aged		
Source of Variation	P value	Significant?
Interaction	ns	No
Age	ns	No
Stimulation	ns	No

Bonferroni posttests- Young vs. Aged				
Age	Difference	t	P value	Summary
Young	0.008615	0.01929	P > 0.05	ns
Aged	0.2416	0.541	P > 0.05	ns

Taz mRNA expression (dCT)				
n	Young Control	Young CCA	Aged Control	Aged CCA
1	11.61	6.70	4.23	6.52
2	10.39	7.14	4.57	4.41
3				
4	2.85	3.37	1.90	2.28
5	6.55	15.68	1.82	1.95
6	3.23	4.32	0.66	0.79
X±SE	6.92±1.79	7.4±2.18	2.63±0.75	3.19±1.02

Two-Way ANOVA- Young vs. Aged		
Source of Variation	P value	Significant?
Interaction	ns	No
Age	*	Yes
Stimulation	ns	No

Bonferroni posttests- Young vs. Aged				
Age	Difference	t	P value	Summary
Young	0.5154	0.295	P > 0.05	ns
Aged	0.5558	0.3182	P > 0.05	ns

ALCAT1 mRNA expression (dCT)				
n	Young Control	Young CCA	Aged Control	Aged CCA
1	4.43	2.88	5.83	3.85
2	6.01	2.21	3.91	3.14
3	3.24	2.84	3.40	5.51
4	3.27	2.70	3.34	3.39
5	4.05	2.73	3.68	2.64
6	4.08	2.34	2.69	3.03
X±SE	4.18±0.41	2.62±0.11	3.81±0.43	3.59±0.41

Two-Way ANOVA- Young vs. Aged		
Source of Variation	P value	Significant?
Interaction	ns	No
Age	ns	No
Stimulation	*	Yes

Bonferroni posttests- Young vs. Aged				
Age	Difference	t	P value	Summary
Young	-1.565	2.918	P < 0.05	*
Aged	-0.2146	0.3999	P > 0.05	ns

MitoPLD mRNA expression (dCT)				
n	Young Control	Young CCA	Aged Control	Aged CCA
1	0.20	0.09	0.28	0.20
2	0.09	0.07	0.07	0.09
3	0.06	0.03	0.04	0.03
4	0.11	0.10	0.07	0.10
5	0.15	0.09	0.09	0.09
6	0.18	0.09	0.07	0.14
X ± SE	0.13 ± 0.02	0.07 ± 0.01	0.10 ± 0.04	0.11 ± 0.02

Two-Way ANOVA- Young vs. Aged		
Source of Variation	P value	Significant?
Interaction	*	Yes
Age	ns	No
Stimulation	ns	No

Bonferroni posttests- Young vs. Aged				
Age	Difference	t	P value	Summary
Young	-0.05628	3.052	P < 0.05	*
Aged	0.004078	0.2211	P > 0.05	ns

Plscr3 mRNA expression (dCT)				
n	Young Control	Young CCA	Aged Control	Aged CCA
1	1.21	2.39	3.04	3.02
2	2.74	4.19	2.33	2.07
3	1.01	1.38	1.31	0.97
4	1.21	2.38	1.38	1.53
5				
6	0.68	4.08	0.75	0.85
X ± SE	1.37 ± 0.32	2.89 ± 0.49	1.76 ± 0.37	1.69 ± 0.36

Two-Way ANOVA- Young vs. Aged		
Source of Variation	P value	Significant?
Interaction	*	Yes
Age	ns	No
Stimulation	ns	No

Bonferroni posttests- Young vs. Aged				
Age	Difference	t	P value	Summary
Young	1.601	3.462	P < 0.05	*
Aged	-0.08365	0.1809	P > 0.05	ns

Table 6: mRNA expression of CL enzymes following denervation and aging

CDS-1 mRNA expression (dCT)				
n	Young Control	Young Denervated	Aged Control	Aged Denervated
1	0.12	0.22	0.15	0.12
2	0.22	0.46	0.11	0.08
3	0.12	0.22	0.11	0.13
4	0.05	0.16	0.14	0.11
5	0.09	0.18	0.30	0.36
6	0.06	0.09	0.10	0.27
X ± SE	0.11 ± 0.02	0.22 ± 0.06	0.15 ± 0.03	0.18 ± 0.05

Two-Way ANOVA		
Source of Variation	P value	Significant?
Interaction	**	Yes
Age	ns	No
Denervation	**	Yes

Bonferroni posttests- Young vs. Aged				
Age	Difference	t	P value	Summary
Young	0.1119	3.627	P<0.01	**
Aged	0.02655	0.8607	P > 0.05	ns

CLS mRNA expression (dCT)				
n	Young Control	Young Denervated	Aged Control	Aged Denervated
1	1.51	2.45	1.12	2.05
2	0.95	1.81	1.29	1.60
3	0.71	1.02	0.71	0.92
4	0.55	0.82	0.88	1.39
5	1.22	1.63	1.00	1.31
6	1.39	2.17	1.22	1.26
X ± SE	1.05 ± 0.15	1.65 ± 2.59	1.03 ± 0.88	1.42 ± 0.15

Two-Way ANOVA		
Source of Variation	P value	Significant?
Interaction	ns	No
Age	ns	No
Denervation	***	Yes

Bonferroni posttests- Young vs. Aged				
Age	Difference	t	P value	Summary
Young	0.5975	4.821	P<0.01	**
Aged	0.3826	3.087	P < 0.05	*

Taz mRNA expression (dCT)				
n	Young Control	Young Denervated	Aged Control	Aged Denervated
1	5.92	4.95	4.12	4.10
2	2.79	3.07	3.14	2.99
3	2.94	2.28	2.76	2.65
4	2.73	3.29	3.56	4.11
5	3.52	4.59	2.86	2.71
6				
X ± SE	3.58 ± 0.55	3.63 ± 0.45	3.29 ± 0.22	3.31 ± 0.30

Two-Way ANOVA		
Source of Variation	P value	Significant?
Interaction	ns	No
Age	ns	No
Denervation	ns	No

Bonferroni posttests- Young vs. Aged				
Age	Difference	t	P value	Summary
Young	0.05587	0.1966	P > 0.05	ns
Aged	0.02729	0.09605	P > 0.05	ns

ALCAT1 mRNA expression (dCT)				
n	Young Control	Young Denervated	Aged Control	Aged Denervated
1	1.55	4.01	1.87	1.75
2	1.84	4.09	2.03	2.14
3	1.21	6.51	1.51	1.76
4	0.42	3.54	0.95	1.39
5	0.49	2.11	0.71	1.20
6	3.35	7.02	0.76	0.65
X ± SE	1.48 ± 0.44	4.55 ± 0.76	1.31 ± 0.23	1.48 ± 0.21

Two-Way ANOVA		
Source of Variation	P value	Significant?
Interaction	***	Yes
Age	*	Yes
Denervation	***	Yes

Bonferroni posttests- Young vs. Aged				
Age	Difference	t	P value	Summary
Young	3.071	7.992	P<0.001	***
Aged	0.1762	0.4585	P > 0.05	ns

MitoPLD mRNA expression (dCT)				
n	Young Control	Young Denervated	Aged Control	Aged Denervated
1	0.027	0.031	0.016	0.027
2	0.013	0.017	0.031	0.009
3	0.009	0.022	0.004	0.013
4	0.017	0.019	0.011	0.018
5	0.007	0.011	0.008	0.005
6	0.014	0.013	0.008	0.009
X ± SE	0.014421 ± 0.002985	0.018930 ± 0.002841	0.013064 ± 0.003978	0.013534 ± 0.003130

Two-Way ANOVA		
Source of Variation	P value	Significant?
Interaction	ns	No
Age	ns	No
Denervation	ns	No

Bonferroni posttests- Young vs. Aged				
Age	Difference	t	P value	Summary
Young	0.004509	1.211	P > 0.05	ns
Aged	0.0004705	0.1263	P > 0.05	ns

Plscr3 mRNA expression (dCT)				
n	Young Control	Young Denervated	Aged Control	Aged Denervated
1	4.092173	4.675187	3.926263	4.591325
2	2.005295	2.131153	2.574178	2.710416
3	2.14033	3.281365	2.010223	2.517745
4	1.723421	2.302112	2.392681	3.142764
5	1.405274	1.750704	1.057099	1.389272
6	1.035019	1.738777	1.166221	1.28445
X ± SE	2.06 ± 0.43	2.6 ± 0.47	2.19 ± 0.43	2.61 ± 0.49

Two-Way ANOVA		
Source of Variation	P value	Significant?
Interaction	ns	No
Age	ns	No
Denervation	***	Yes

Bonferroni posttests- Young vs. Aged				
Age	Difference	t	P value	Summary
Young	0.005796	4.613	P<0.01	**
Aged	0.004182	3.328	P < 0.05	*

Table 7: mRNA expression of CL metabolism enzymes in PGC-1α knockout mice.

CDS-1 mRNA expression (dCT)		
n	**Wildtype**	**Knockout**
1	0.16	0.10
2	0.23	0.09
3	0.51	0.16
4	0.46	0.15
5	0.39	0.13
6	0.27	0.10
7	0.20	0.08
X ± SE	**0.32 ± 0.05**	**0.12 ± 0.01**

Unpaired t test
Wildtype vs. Knockout
Two-tailed P value = 0.0023
t = 5.053
df = 6

CLS mRNA expression (dCT)		
n	**Wildtype**	**Knockout**
1	5.20	8.11
2	8.72	7.12
3	9.78	11.45
4	11.79	11.08
5	9.07	10.90
6	11.59	8.40
7	10.58	14.85
X ± SE	**9.53 ± 0.85**	**10.27 ± 0.99**

Unpaired t test
Wildtype vs. Knockout
Two-tailed P value = 0.58
t = 0.5666
df = 12

Taz mRNA expression (dCT)		
n	**Wildtype**	**Knockout**
1	12.43	13.21
2	13.79	12.56
3	27.35	29.28
4	35.38	32.79
5	139.48	160.00
6	167.98	117.55
7	26.24	28.36
X ± SE	**60.38 ± 24.49**	**56.25 ± 22.01**

Unpaired t test
Wildtype vs. Knockout
Two-tailed P value = 0.90
t = 0.1254
df = 12

ALCAT1 mRNA expression (dCT)		
n	Wildtype	Knockout
1	1.11	3.26
2	1.03	2.39
3	1.20	1.56
4	1.55	3.90
5	2.84	4.31
6	2.90	3.47
7	1.77	3.59
X ± SE	1.77 ± 0.30	3.21 ± 0.35

Unpaired t test
Wildtype vs. Knockout
Two-tailed P value = 0.009
t = 3.098
df = 12

MitoPLD mRNA expression (dCT)		
n	Wildtype	Knockout
1	0.06	0.07
2	0.19	0.14
3	0.85	0.47
4	0.60	0.44
5	1.18	1.44
6	2.26	1.67
7	1.10	1.01
X ± SE	0.89 ± 0.28	0.75 ± 0.24

Unpaired t test
Wildtype vs. Knockout
Two-tailed P value = 0.70
t = 0.3889
df = 12

Plscr3 mRNA expression (dCT)		
n	Wildtype	Knockout
1	6.93	7.48
2	9.54	7.15
3	22.22	24.64
4	27.33	23.98
5	17.08	20.73
6	19.61	17.49
7	10.28	11.36
X ± SE	16.14 ± 2.84	16.12 ± 2.83

Unpaired t test
Wildtype vs. Knockout
Two-tailed P value = 0.99
t = 0.005
df = 12

Table 8: Relative mRNA levels of CL metabolism enzymes in rat.

mRNA levels in rat muscle (dCT)						
n	CDS-1	CLS	Taz	ALCAT1	MitoPLD	Plscr3
1	0.007	2.565	4.588	4.429	0.104	3.606
2	0.004	1.387	8.529	6.007	0.174	4.243
3	0.006	1.472	9.875	3.244	0.081	3.916
4	0.004	1.055	1.706	3.415	0.094	1.299
5	0.005	1.272	1.908	3.050	0.468	1.730
6	0.004	1.298	2.733	3.084	0.105	1.340
7	0.015	1.105	5.472	2.001	0.020	2.999
8	0.035	1.189	3.422	2.311	0.165	2.522
9	0.184	0.764	2.443	1.689	0.094	2.314
10	0.040	0.859	2.749	0.406	0.265	2.711
11	0.069	1.261	1.499	0.384	0.069	1.452
12	0.015	0.858	1.164	0.880	0.086	0.640
X ± SE	0.03 ± 0.01	1.26 ± 0.14	3.84 ± 0.81	2.57 ± 0.48	0.14 ± 0.03	2.40 ± 0.33

	ANOVA Table	SS	df	MS
One way analysis of variance	Between	282	6	47.01
Control vs. 7 day CCA	Within	206.2	77	2.678
P value < 0.0001	Total	488.2	83	

Tukey's Multiple Comparison Test	Mean Diff.	q	P value
CDS-1 vs CLS	-1.225	2.592	P > 0.05
CDS-1 vs Taz	-3.808	8.062	P < 0.001
CDS-1 vs ALCAT1	-2.543	5.382	P < 0.01
CDS-1 vs MitoPLD	-0.1114	0.2359	P > 0.05
CDS-1 vs Plscr3	-2.365	5.007	P < 0.05
CLS vs Taz	-2.584	5.469	P < 0.01
CLS vs ALCAT1	-1.318	2.79	P > 0.05
CLS vs MitoPLD	1.113	2.357	P > 0.05
CLS vs Plscr3	-1.14	2.414	P > 0.05
Taz vs ALCAT1	1.266	2.679	P > 0.05
Taz vs MitoPLD	3.697	7.826	P < 0.001
Taz vs Plscr3	1.443	3.055	P > 0.05
ALCAT1 vs MitoPLD	2.431	5.146	P < 0.01
ALCAT1 vs Plscr3	0.1775	0.3756	P > 0.05
MitoPLD vs Plscr3	-2.254	4.771	P < 0.05

Table 9: Relative mRNA levels of CL metabolism enzymes in mouse.

mRNA levels in mouse muscle (dCT)						
n	CDS-1	CLS	Taz	ALCAT1	MitoPLD	Plscr3
1	4.814	48.475	115.955	10.321	0.527	64.610
2	7.233	74.283	102.278	8.806	1.578	81.287
3	13.263	171.218	478.599	21.001	14.826	388.729
4	15.622	175.923	527.762	23.177	8.948	407.765
5	16.311	109.352	1680.761	34.224	14.164	205.838
6	9.583	114.074	1653.444	28.525	22.260	193.018
7	10.597	178.577	442.776	29.890	18.633	173.390
X ± SE	11.06 ± 1.61	124.56 ± 19.76	714.51 ± 254.12	22.29 ± 3.67	11.56 ± 3.12	216.38 ± 51.20

	ANOVA Table	SS	df	MS
One way analysis of variance	Between	0.2381	5	0.04761
Control vs. 7 day CCA	Within	0.1384	36	0.003846
P value < 0.0001	Total	0.3765	41	

| Tukey's Multiple Comparison Test	Mean Diff.	q	P value
CDS-1 vs CLS	-0.1135	0.9955	P > 0.05
CDS-1 vs TAZ	-0.7442	6.528	P < 0.001
CDS-1 vs ALCAT1	-0.01122	0.09839	P > 0.05
CDS-1 vs MitoPLD	-0.0005018	0.004401	P > 0.05
CDS-1 vs Plscr3	-0.2053	1.801	P > 0.05
CLS vs TAZ	-0.6307	5.532	P < 0.01
CLS vs ALCAT1	0.1023	0.8971	P > 0.05
CLS vs MitoPLD	0.113	0.9911	P > 0.05
CLS vs Plscr3	-0.09182	0.8054	P > 0.05
TAZ vs ALCAT1	0.733	6.429	P < 0.001
TAZ vs MitoPLD	0.7437	6.523	P < 0.001
TAZ vs Plscr3	0.5389	4.727	P < 0.05
ALCAT1 vs MitoPLD	0.01072	0.09399	P > 0.05
ALCAT1 vs Plscr3	-0.1941	1.703	P > 0.05
MitoPLD vs Plscr3	-0.2048	1.796	P > 0.05

# Appendix B

Experimental protocols

Implantable stimulation unit-surgical procedure

Sterilize all surgical tools prior to commencing the surgical procedures outlined below and also keep lab bench as sterile as possible by wiping it down thoroughly with ethanol.

1. Shave the skin over the left flank (between the last rib and the pelvis) and over the left hindlimb and wipe with iodine.
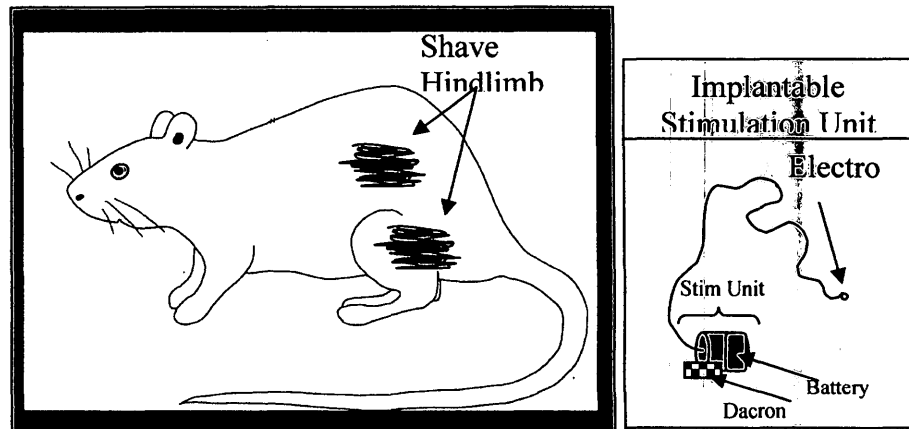

2. Make a skin incision midway between the most distal rib and the pelvic girdle with the rat lying on its side in a vertical direction that extends from approximately 30-40% (10-20mm) of the circumferential distance from the umbilicus to the spine (the strategy is to make the incision far enough from the spine to penetrate the less complex musculature but to try to minimize the extent of the incision on the ventral surface of the animal to avoid post-surgery dragging of the wound during locomotion).
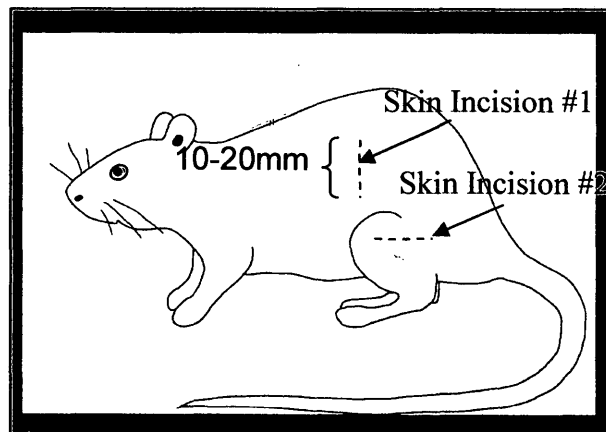
3. Tunnel a subcutaneous passage from the left hindlimb to the left flank using the tunneler.


Subcutaneous Tunneling
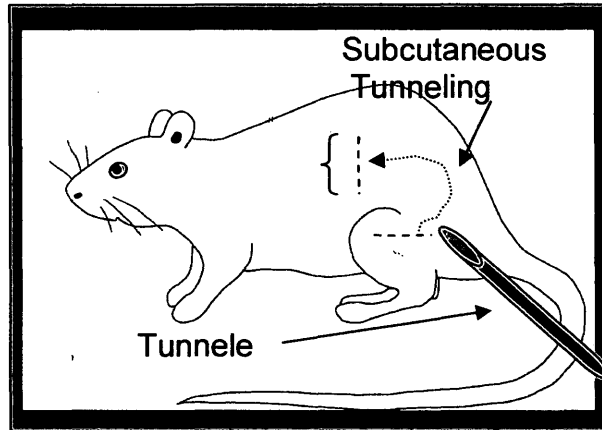
Tunnele

4. Once the skin incision has been made on the left flank tunneling has been performed, lift the abdominal wall (with forceps) and snip horizontally through the abdominal musculature. This incision only needs to be large enough for the stimulation unit to be squeezed through but keep the Dacron mesh upwards, so that it can be incorporated into the suture line that closes the abdominal musculature.

Horizontal Muscle
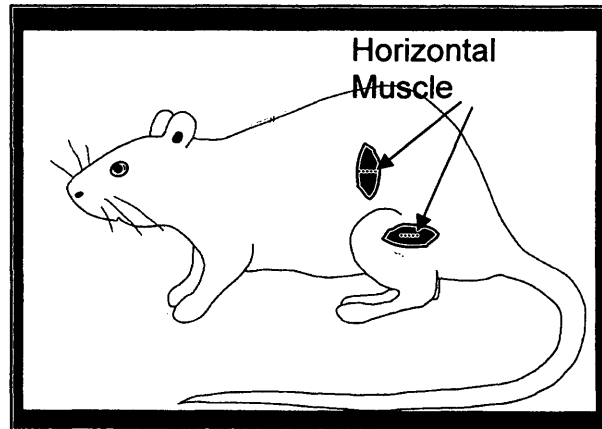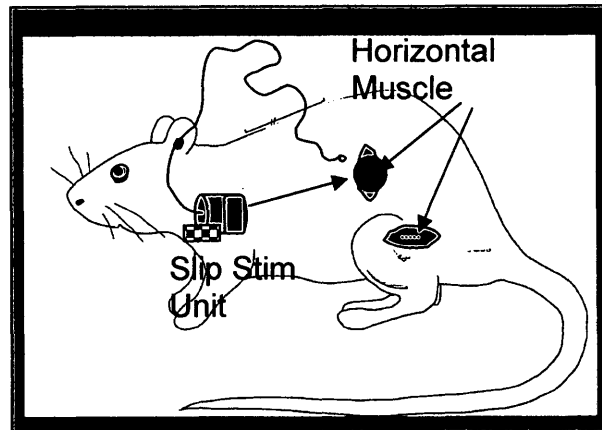
5. Suture the abdominal wall with 5.0 silk and incorporate the Dacron mesh into the suture line (about 3-4 independent sutures). Keep the electrodes to one side of the suture line.
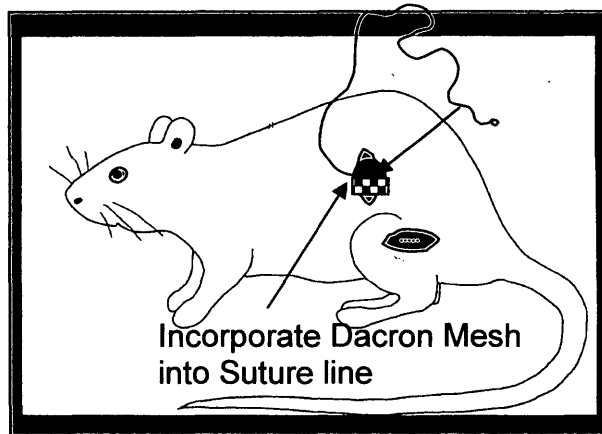
6. Affix the electrodes to the tunneler by folding over the end-piece (one with the slot) of the tunneler and carefully tunnel the electrodes from the left flank to the left hindlimb being sure not to damage the electrodes.

7. Make small horizontal cut into the underlying left hindlimb muscle (biceps femoris) and blunt through the muscle to expose the peroneal nerve (exactly the same as our external stimulation protocol). Once the nerve has been exposed, use 4 retractors gain a larger exposure of the nerve and underlying musculature.

8. Electrodes contain a loop on the end of the lead. Place needle of suture through the loop and tie a knot that attaches the suture to the loop of the electrode.

8. Using forceps (with sharp teeth), pinch a small amount (between 0.5-1.0 mm) of muscle that is flanking the peroneal nerve. Place needle through the pinched muscle

section and proceed to tie down the loop section of the electrode to the underlying muscle. Once the loop section has been tied down, tie down a proximal section (3-4mm from the electrode loop) of the electrode to another thin section of muscle that is 3-4mm away from the loop portion.

9. Repeat steps 7 and 8 for the other electrode lead but suture this electrode on the other side of the peroneal nerve. Test the stimulation unit by turning the unit on with the digital stroboscope (ON-2 Flashes, OFF-1 Flash). Palpate the muscle to ensure adequate stimulation.

10. Once both electrodes are sutured to the underlying muscle, the incision is closed with 3-5 independent sutures (5.0 silk) and the skin closure is stapled.

Surgery for denervation of skeletal muscle

1. Sterilize surgical instruments in autoclave machine for 20 minutes.
2. Anaesthetize rat with 0.2 mls/100g body weight of Ketamine/Xylazine.
3. Shave animal's right hindlimb close to the skin.
4. Wipe the shaved area with 1% topical iodine antiseptic solution.
5. Make a 2 cm incision in the skin approximately 1 cm posterior and 1 cm inferior to the knee.
6. Carefully blunt dissect through the exposed superficial muscle until the common peroneal nerve is visualized. This nerve innervates the tibialis anterior (TA) and extensor digitorum longus (EDL) muscles.
7. Cut out a small 5mm section of the nerve. This ensures that the nerve endings will not regenerate during the experiment and thus effectively denervates the TA and EDL muscles.
8. Inject a small volume (~0.1mls) of sterile ampicillin in the local incision site.
9. Using the 5.0 surgical silk, suture close the superficial muscle tear. Seal the overlying skin on the hindlimb using surgical staples.
10. Monitor the animal over the next 24 hours to ensure recovery. The animal is free to move about the cage and feed/drink *ad libitum.*
11. Recovering animals are given amoxicillin in their drinking water (0.025% w/v) for 1 week after surgery.

98
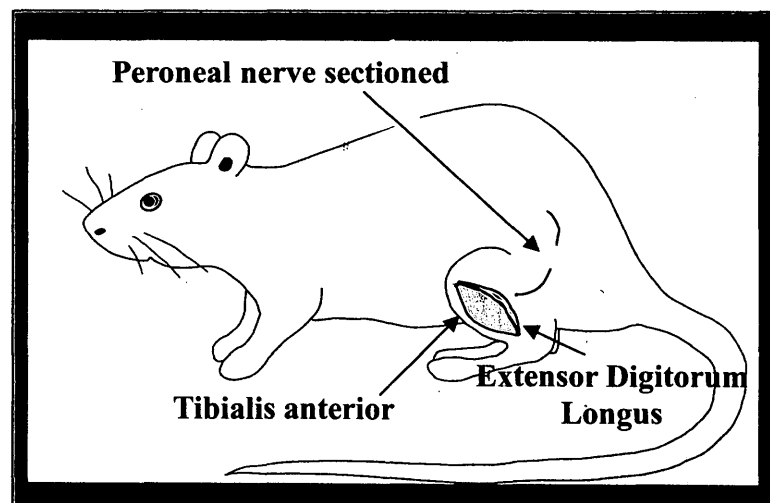
Cytochrome c oxidase (COX) assay for microplate reader

Theory

Cell extract containing cytochrome c oxidase is added to the test solution containing fully reduced cytochrome c. The rate of cytochrome c oxidation is measured over time as a reduction in absorbance at 550 nm. The reaction is carried out at 30° C.

Reagents

1. Horse Heart Cytochrome c (Sigma, C-2506)
2. Sodium Dithionite
3. 100 mM K-Phosphate Buffer (KPO_4; pH to 7.0)
   -make and mix equal proportions of 0.1 M KH_2PO_4 and 0.1 M $K_2HPO_4.3H_2O$
4. 10 mM K-Phosphate Buffer
   -dilute 100 mM K-Phosphate Buffer 1:10 with ddH_2O

Procedure

1. Immediately following the completion of the enzyme extraction protocol from cells, proceed to making Test Solution. Add the following to a scintillation vial:

- weigh out 20 mg of horses heart cytochrome c
- add 1 ml of 10 mM KPO_4 buffer and fully dissolve cytochrome c
- make up a small volume of 10 mg/ ml sodium dithionite- 10 mM KPO_4 stock solution (Note: make fresh each experiment and use within 20 minutes)
- add 40 µl of dithionite stock solution to the Test Solution and observe the red to orange colour change
- add 8 ml of ddH_2O
- add 1 ml of 100 mM KPO_4 buffer (Note: the Test Solution becomes light sensitive at this step; make sure to the cover vial with aluminum foil).

2. Add 300 µl of Test Solution into 4-8 wells of a 96-well microplate and incubate at 30°C for 10 minutes to stabilize the temperature and absorbance.

1. Open KC4 plate reader program. Select CONTROL icon, then PRE-HEATING tab, enter 30°C and select ON (Do not run assay until KC4 temperature has reached 30°C).
2. Set-up of COX activity protocol on computer.

3. Select WIZARD icon, then READING PARAMETERS icon.

- Select Kinetic for Reading Type.
- Select Absorbance for Reader and 550 nm for wavelength (drop-down).
- Select Sweep for Read Mode.
- Select 96 Well Plate (default) for Plate Type.
- Enter first and last well to be read (eg. A1 and A4 if reading 4 samples simultaneously).
- Select Yes and Pre-heating and enter 30 for Temperature Control.
- For Shaking enter 0 for both intensity and duration (shaking is not necessary and it will delay the first reading).
- Do not select either of the two options for Pre-reading.
- Click on the KINETIC... rectangular tile to open the Kinetic window.
- Enter run time (1 minute is recommended) and select MINIMUM for Interval time (under these conditions the minimum Interval time should be 3 seconds).
- Select Allow Well Zoom During Read to see data in real time (optional).
- Under Scales, checkmarks should appear for both Auto check boxes. Do not select Individual Well Auto Scaling.
- Press OK to return to Reading Parameters window. Press OK to return to Wizard window. Press OK. Do not save the protocol.

4. Set the micropipette to 225 μl and secure 4-8 tips on the white projections (make sure they are on tight and all the same height).

5. In a second, clean 96 well plate, pipette samples into 4-8 empty wells (start with A1). *Recommended volumes:* 65 μl of enzyme extract from C2C12 cells.

6. Remove microplate with Test Solution from the incubator (as long as it has been incubating for 10 minutes). Place this plate beside the plate with the sample extracts in it.

7. On KC4 program, select the READ icon and press the START READING icon, then press the READ PLATE button. A box will appear that says, "Insert plate and start reading". Do not press OK yet, but move the mouse so that the cursor hovers over the OK button.

8. Using the micropipette (set to 225 μl) carefully draw up the Test Solution. Make sure the volume is equal in all the pipette tips, and that no significant air bubbles have entered any of the tips.

9. Pipette the Test Solution into the wells with the sample extracts (the second plate). As soon as all the Test Solution has been expelled from the tips (do not wait for the second push from the multipipette), place the plate onto the tray of the plate

reader and with the other hand on the mouse, press the OK button. (Speed at this point is paramount, as there is an unavoidable latency period between the time of pressing the OK button and the time of the first reading.)

10. If desired, add 5 μl KCN to one of the wells to measure any absorbance changes in the presence of the CYTOX inhibitor.

11. Once reading is complete, hold the CTRL key on the keyboard, and use the mouse to click once on each of the squares corresponding to a well that had sample in it. Once all the desired wells have been highlighted by a black square (up to a maximum of 8 wells), let go of the CTRL key and a large graph will appear with lines on it representing each sample.

12. To obtain the rate of change of absorbance over different time periods, select Options and enter the amount of time for which you would like a rate of change of absorbance to be calculated. The graph, along with one rate (at whichever time interval is selected) for each sample can be printed on a single sheet of paper, and the results can be saved.

13. The delta absorbance will appear in units of mOD/min and the number given will be negative. Convert this to OD/min by dividing by 1000 and omit the negative sign in the calculation. (eg. if Mean V: -394.8 mOD/mn, then use 0.395 OD/min)

CALCULATION:

$$\text{CYTOX activity} = \frac{\text{mean dealta absorbance/ minute x total volume (ml) x 1000}}{18.5 \ (\mu\text{mol/ml extinction coeff.}) \times \text{sample volume (ml)} \times \text{total } \mu\text{g/ well}}$$

Example Calculation:

55 μl of enzyme extraction
230 μl of Test Solution
Mean V: -584.30 mOD/mn
Protein concentration: 3.023 μg/ μl
Total μg/ well: 151.15

$$\text{COX activity} = \frac{(0.5843)(0.285)(1000)}{(18.5)(0.055)(3.023 \times 55)}$$

COX activity = 0.967 nmol/min/μg protein

Mitochondrial isolation

Reagents
All buffers are set to pH 7.4 and stored at 4 °C

- Buffer 1
  - 100 mM KCl
  - 5 mM MgSO4
  - 5 mM EDTA
  - 50 mM Tris base

- Buffer 1 + ATP
  - Add 1 mM ATP to Buffer 1

- Buffer 2
  - 100 mM KCl
  - 5 mM MgSO4
  - 5 mM EGTA
  - 50 mM Tris base
  - 1 mM ATP

- Resuspension medium
  - 100 mM KCl
  - 10 mM MOPS
  - 0.2% BSA

- Nagarse protease (Sigma, P-4789)
  - 10 mg/ml in Buffer 2
  - Make fresh for each isolation, keep on ice

Procedure

1. Remove the tibialis anterior (TA) muscle from the rat, and put it in a beaker containing 5 ml Buffer 1, on ice immediately.
2. Place TA on a watch glass that is also on ice and trim away fat and connective tissue. Proceed to thoroughly mince the muscle sample with forceps and scissors, until no large pieces are remaining.
3. Place the minced tissue in a plastic centrifuge tube and record the exact weight of tissue.
4. Add a 10-fold dilution of Buffer 1 + ATP to the tube.
5. Homogenize the samples using the Ultra-Turrax polytron with 40% power output and 10 s exposure time. Rinse the shaft with 0.5 ml of Buffer 1 + ATP to help minimize sample loss.
6. Using a Beckman JA 25.50 rotor, spin the homogenate at a centrifuge setting of 800 g for 10 min. This step divides the IMF and SS mitochondrial subfractions. The supernate will contain the SS mitochondria and the pellet will contain the IMF mitochondria.

SS mitochondrial isolation:

7. Filter the supernate through a single layer of cheesecloth into a second set of 50 ml plastic centrifuge tubes.
8. Spin tubes at 9000 g for 10 min. Upon completion of the spin discard the supernate and gently resuspend the pellet in 3.5 ml of Buffer 1 + ATP. Since the mitochondria are easily damaged, it is important that the resuspension of the pellet is done carefully.
9. Repeat the centifugation of the previous step (9000 g for 10 min) and discard the supernate.
10. Resuspend the pellet in 200 µl of Resuspension medium, being gentle so as to prevent damage to the SS mitochondria. Some extra time is needed during this final resuspension to ensure the SS pellet is completely resuspended.
11. Keep the SS samples on ice while proceeding to islolate the IMF subfraction.

IMF mitochondrial isolation:

7. Gently resuspend the pellet (from step 6) in a 10-fold dilution of Buffer 1 + ATP using a teflon pestle.
8. Using the Ultra-Turrax polytron set at 40% power output, polytron the resuspended pellet for 10 s. Rinse the shaft with 0.5 ml of Buffer 1 + ATP.
9. Spin at 800 g for 10 min and discard the resulting supernate.
10. Resuspend the pellet in a 10-fold dilution of Buffer 2 using a teflon pestle.
11. Add the appropriate amount of nagarse. The calculation for the appropriate volume is 0.025 ml/g of tissue. Mix gently and let stand exactly 5 min.
12. Dilute the nagarse by adding 20 ml of Buffer 2.
13. Spin the diluted samples at 5000 g for 5 min and discard the resulting supernate.
14. Resuspend the pellet in a 10-fold dilution of Buffer 2. Gentle resuspension is with a teflon pestle.
15. Spin the samples at 800 g for 10 min. Upon the completion of the spin, the supernate is poured into another set of 50 ml plastic tubes (on ice), and the pellet is discarded.
16. Spin the supernate at 9000 g for 10 min. The supernate is discarded and the pellet is resuspended in 3.5 ml of Buffer 2.
17. Spin samples at 9000 g for 10 min and discard the supernate.
18. Gently resuspend the pellet in 300 µl of Resuspension medium.

Bradford protein assay

Reagents

- Extraction buffer
  - 100 mM Na/K PO$_4$
  - 2 mM EDTA
  - pH to 7.2

- 5 X Bradford dye
  - 250 ml 85% Phosphoric acid
  - 250 ml 100% Ethanol
  - 500 ml ddH$_2$O
  - 0.235 g Coomassie Brilliant Blue G250

- Bovine Serum Albumin (BSA)
  - 2 mg/ml in ddH$_2$O

Procedure

1. Prepare the test tubes allowing for duplicates of each sample.
2. Add 95 µl of extraction buffer to each tube.
3. Add 5 µl of sample to each tube containing the extraction buffer.
4. To generate the standard curve, add the following volumes (in µl) of extraction buffer: BSA, each in separate tubes – 100:0, 95:5, 90:10, 85:15, 80:20, 75:25.
5. Pipette 5 ml of 1 X Bradford reagent into each tube and mix by gentle vortexing.
6. In duplicate, add 0.2 ml of each test tube to 96 well plate wells.
7. Measure absorbance of wells at 595 nm with a microplate reader.
8. Calculate the protein concentration of each sample using the standard curve.

Flow cytometry

Reagents

Resuspension Buffer
       100 mM KCl
       10 mM MOPS
   0.2% BSA

5 μM NAO solution
       2.5 μL of 1 mM NAO
       500 μL of resuspension buffer

Procedure

1. Obtain 100 mg of isolated mitochondria
   a. Spin down at 9000 g for 3 minutes at room temperature
   b. Dump supernatant fraction
   c. Resuspend in 500 μL of 5 μ NAO
   d. Leave at room temperature for 15 minutes

2. Wash
   a. Spin down at 9000 g for 3 minutes at room temperature
   b. Dump supernatant fraction
   c. Resuspend in 300 μL of resuspension buffer

Samples now ready for Flow Cytometer, observed at 50 000 events.

Gating:
Mitochondrial population
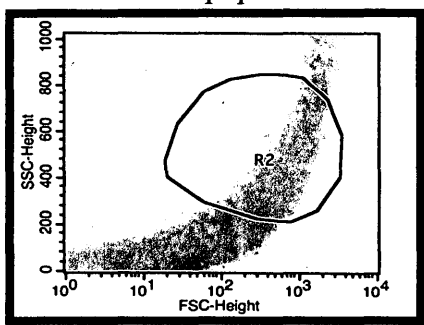
Histogram:
Fluorescence of NAO stain
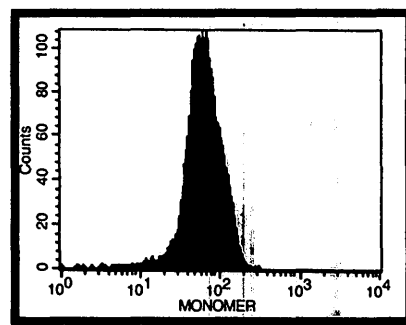
The mitochondrial dye MitoTracker Green FM was used to discriminate between mitochondria and debris, and thus gate the R2 region.

RNA Isolation

Procedure

1) Homogenize (approximately 30 sec. @ 30-40% power) tissues (200 mg) at 30% in 2 ml Tri-reagent in a 13 ml Sarstedt tube;

<div align="center">OR</div>

Homogenize (approximately 30 sec. @ 30-40% power) tissues (200 mg) at 30% in 1.25 ml solution D + 1.25 ml phenol + 0.125 ml 2M sodium acetate (pH 4.0) in a 13 ml Sarstedt tube

   **Note: The homogenizer must be sterilized in 0.1M NaOH and rinsed in sterile water prior to use. Rinse in sterile water between samples.

2) Let stand for 5 min at room temperature;

3) Add 0.4 ml chloroform and shake vigorously for 15 sec, let stand for 2-3 min at room temperature;

4) Spin at 12,000 g for 15 min at 4°C;

5) Transfer aqueous phase to 13 ml Sarstedt tube;

6) Add 1 ml isopropanol, gently shake, and allow precipitation of RNA for 5-10 min at room temperature;

7) Spin at 12,000 g for 10 min at 4°C;

8) Remove supernatant fraction and add 0.7 ml 75% ethanol;

9) Transfer RNA to eppendorf tube;

10) Rinse 13 ml Sarstedt tube with 0.3 ml 70% ethanol, add to eppendorf tube and mix by vortexing;

11) Spin 5 min in eppendorf centrifuge at 4°C;

12) Discard supernatant fraction;

13) Dry pellet under a vacuum in dessicator (DO NOT DRY PELLET WITH CENTRIFUGATION UNDER A VACUUM);

14) Dissolve pellet in 50-200 µl sterile distilled DEPC water and measure absorbance at 260 nm and 280 nm.

Reagents

1. *Solution D (Denaturing solution)*

4 M Guanidinium Thiocyanate	125 g
25 mM of 1 M stock NaCitrate (pH 7.0)	6.6 ml
N-Lauroyl Sarcosine;Sigma L-5125 (0.5% Sarcosyl)	1.32 g
ddH$_2$O	160 ml

        **Note: make up solution D and store at RT for up to 3 months. On the day of the experiment, mix 50 ml of Solution D with 0.36 ml of beta-Mercaptoethanol (0.1 M b-MEtOH)

2. *Phenol (Nucleic acid grade)*
   a) Melt solid phenol at 68 °C (cap loose) in H$_2$O;
   b) Add 0.25 g 8-hydroxyquinoline to 250 ml of phenol, mix;
   c) Add 250 ml 1.0 M Tris HCl (pH 8.0) and stir overnight at 4 °C covered in foil
   d) Remove supernatant fraction;
   e) Add 250 ml 0.1 M Tris-HCl containing 0.2 % b-MEtOH (0.178 ml/100 ml for S.G. = 1.12) and mix thoroughly;
   f) Allow solution to settle and remove supernatant fraction;
   g) Repeat 2 more times as above or until pH of phenol is > 7.6 (test with pH paper).
   h) Store in 25-50 ml aliquots at -20 °C.

3. *2.0 M Na Acetate* (pH 4.0)
   10.88 g/100 ml sterile H$_2$O

4. *75% ethanol in sterile H$_2$O*
   (75 ml ethanol + 25 ml dH$_2$O)

RNA formaldehyde gel

Reagents

1. *0.1% SDS (Sodium Dodecyl Sulfate)*

2. *10x MOPS (Morpholinepropanesulfonic acid)*
   41.86 g MOPS
   3.72 g EDTA
   900 ml dH$_2$O, pH to 7.4
         * make up to 1 L, autoclave

3. *Agarose*

4. *Sterile ddH$_2$O*

5. *0.5 mg/ml EtBr (Ethidium Bromide)*

6. RNA Sample Buffer
   100% deionized formamide
   37% formaldehyde
   1M MOPS (pH 7.4)
   0.5M EDTA
   100% glycerol
   1% dyes (10 mg bromphenol blue, 10mg Xylene Cyanol)
   10% SDS

Procedure

1. Prepare the gel and electrophoresis chamber after overnight or 1 hr sterilization with 0.1% SDS;

2. Rinse the gel plates, electrophoresis chamber, and comb with sterile ddH$_2$O, and wipe dry;

   Running buffer:

Small Chamber	Large Chamber
30 ml 10X MOPS	200 ml 10X MOPS
270 ml Sterile ddH$_2$O	1800 ml Sterile ddH$_2$O

   1% Agarose gel:

Small Gel	Large Gel
0.4 g Agarose	1.7 g Agarose
4 ml 10 X MOPS	17 ml 10 X MOPS
34ml Sterile ddH$_2$O	144 ml Sterile ddH$_2$O
Weigh, melt, make up volume with sterile ddH$_2$O weight and add:	
2 ml 37% Formaldehyde	8.5 ml 37% Formaldehyde

3. Allow gel to cool for 15 minutes, pour, and let gel set for 30 min. Transfer the plate with the gel to an electrophoresis chamber, and place the end with the wells at the negative electrode;

4. Calculate the volumes of RNA and sample buffer required for desired amount of RNA;

   Combine in sterile eppendorf tubes:
   RNA.. x μl
   EtBr.. 4 μl
   Sample buffer.................................. x μl

*Note: use at least a 1:1 ratio of buffer to RNA volume. (max. volume of 30 µl).

5. Mix the samples by tapping;

6. Denature the samples for 65°C for 10 min, quick cool;

7. Spin down volume briefly in microfuge;

8. Pipette the entire volume into each well of the gel.

9. Run the gel (~80 V) until second dye band, Xylene Cyanol, is 2/3 from the end;

10. Visualize and photograph the gel under UV light.

Reverse transcription: first strand cDNA synthesis

First-strand cDNA synthesis is performed following the manufacturer's recommendations that are outlined below:

Reagents

1. total RNA (isolated as described)
2. Oligo(dT)$_{12-18}$
3. 10 mM dNTPs (dATP, dTTP, dCTP, dGTP; 10 mM each)
4. Sterile ddH$_2$0
5. RNAse OUT (40 units/ μl)
6. 0.1 M DTT
7. 5X First-strand Buffer
8. SuperScript II RT

*Note: All reagents except RNA are supplied with the SSII kit from Invitrogen.

Procedure

1. Add following components to a nuclease/ RNA-free 500 μl eppendorf:

Oligo(dT)$_{12-18}$	1μl
1 μg of RNA	x μl
dNTP mix	1 μl
Sterile ddH$_2$0	to 20 μl

2. Heat mixture to 65°C for 5 minutes and quick chill on ice. Collect the contents with a quick spin in a tabletop microcentrifuge and then add:

5X First-strand buffer	4 μl
0.1 M DTT	2 μl
RNAse OUT	1 μl

3. Mix contents of tube gently and incubate at 42°C for 2 minutes.
4. Add 1 μl (200 units) of Superscript II RT and mix by pipetting gently up and down.
5. Incubate at 42°C for 50 minutes.
6. Inactivate the reaction by heating at 70°C for 15 minutes.
7. cDNA is ready for use in PCR amplification.

Real-time polymerase chain reaction (PCR)

1.   Convert 2 ug of RNA to 2 ug of cDNA (STOCK cDNA)
2.   Diluted STOCK cDNA to 1:30 (WORKING cDNA)
        -2 uL STOCK cDNA + 58 uL nuclease-free ddH$_2$O
3.   Add 10 µg cDNA per well (4 µL of WORKING cDNA)

For SYBR Green analyses
    1. Primers were diluted to 300 µM (STOCK primers),
    2. Diluted further to 20 µM (WORKING primers) in a separate tube;
    3. In each well, add
        -   2.5 µL of both forward and reverse primers;
        -   12.5 µL Quanta PerfeCTa SYBR® Green SuperMix, ROX Master Mix;
        -   3.5 µL nuclease-free ddH$_2$O;
        -   4 µL of WORKING cDNA.

For TaqMan analyses
    1. In each well, add
        -   12.5 µL TaqMan Universal Master Mix;
        -   1.25 µL the appropriate TaqMan probes;
        -   7.25 µL nuclease-free ddH$_2$O;
        -   4 µL of WORKING cDNA.

Total reaction volumes is 25 µL per well.

Duplicated samples to ensure accuracy.

Use negative wells to monitor contamination (nuclease-free ddH$_2$O in place of cDNA).

Check for nonspecific amplification and primer dimers by analyzing melt curves

Gene, Size (bp)	Type	Accession Number	Forward Primer	Reverse Primer
CDS-1	Rat	NM_031242.2	Applied Biosystems TaqMan Probe Assay ID Rn00579942_m1	
Lclat1 (ALCAT1)	Rat	XM_343020.4	Applied Biosystems TaqMan Probe Assay ID Rn01468447_m1	
Rps12	Rat	NM_031709.3	Applied Biosystems TaqMan Probe Assay ID Rn01789993_u1	
Myc	Rat	NM_012603.2	Applied Biosystems TaqMan Probe Assay ID Rn00561507_m1	
Gapdh	Rat	NM_017008.13	Applied Biosystems TaqMan Probe Assay ID Rn01775763_g1	
β-Actin	Rat	NM_031144.2	Applied Biosystems TaqMan Probe Assay ID Rn00667869_m1	
Crls1 (CLS), 66	Rat	NM_001014258.1	5'-AAT GTT GAT CGC TGC TGT GTT T-3'	5'-TTA GCT AGT GTT CGC GGT GTT G-3'
Taz, 63	Rat	NM_001025748.1	5'-CGG CTG ATT GCT GAG TGT CA-3'	5'-TCA TTC ATT CCA ACA TGC CAT AG-3'
Pld6 (MitoPLD) 116	Rat	XM_220517.3	5'-TCA TCA CGG ACT GCG ACT A-3'	5'-GGC AAA CTT ATG GTG CAT GT-3'
Plscr3, 120	Rat	NM_001012139.2	5'-GCA CCA AAG ATG GCA GAT A-3'	5'-TAA TAG CTG TAG GGT TGG GAC C-3'
Myc, 123	Rat	NM_012603.2	5'-GCT CTG CTC TCC GTC CTA TGT-3'	5'-ATG ACC GAG CTA CTT GGA GG-3'
Rps12, 127	Rat	NM_031709.3	5'-ATG GAC GTC AAC ACT GCT CT-3'	5'-ATCTCT GCG TGC TTG CAT-3'
Gapdh, 122	Rat	NM_017008.3	5'-CTC TCT GCT CCT CCC TGT TCT A-3'	5'-GGT AAC CAG GCG TCC GAT AC-3'
β-Actin, 154	Rat	NM_031144.2	5'-CCC CAT TGA ACA CGG CAT T-3'	5'-GCC AAC CGT GAA AAG ATG ACC-3'
CDS-1	Mouse	NM_173370.3	Applied Biosystems TaqMan Probe Assay ID Mm01208328_m1	
B2M	Mouse	NM_009735.3	Applied Biosystems TaqMan Probe Assay ID Mm00437762_m1	
β-Actin	Mouse	NM_007393.3	Applied Biosystems TaqMan Probe Assay ID Mm00607939_s1	
Gapdh	Mouse	NM_008084.2	Applied Biosystems TaqMan Probe Assay ID Mm99999915_g1	
Crls1, 107	Mouse	NM_001024385.1	5'-GGT GTT GCACAGCATTCA-3'	5'-GCT GGA TCT GGG TGC TTC T-3'
Taz, 205	Mouse	NM_001173547.1	5'-CCC TCC ATG TGA AGT GGC CAT TCC-3'	5'-TGG TGG TTG GAG ACG GTG ATA AGG-3'
Lclat1 (ALCAT1) 111	Mouse	NM_001081071.2	5'-AGC TGT TTG ACT CCC TAG T-3'	5'-TGA TCC ATC AGA GAA ACT TA-3'
Pld6, (MitoPLD) 127	Mouse	NM_183139.2	5'-CAC AAG TTT GCC ATC GTT GA-3'	5'-GGA ACA GCC GCA CAT ACT-3'
Plscr3, 100	Mouse	NM_023564.4	5'-CTG ATC GCC AAC CTG TTC TA-3'	5'-CTT CGC GAT TCA TCC TTA GT-3'
B2M, 106	Mouse	NM_009735.3	5'-GGT CTT TCT GGT GCT TGT CT-3'	5'-TAT GTT CGG CTT CCC ATT CT-3''
β-Actin, 117	Mouse	NM_007393.3	5'- TGT GAC GTT GAC ATC CG TAA—3''	5'- GCT AGG AGC CAG AGC AGT AA—3''
Gapdh, 113	Mouse	NM_008084.2	5'-AAC ACT GAG CAT CTC CCT CA-3''	5'-GTG GGT GCA GCG AAC TTT AT—3''

Appendix C

Other Contributions to Literature

Other Contributions to Literature

Publications

4. **Ostojic O**, O'Leary MFN, Singh K, Menzies KJ and Hood DA. The effects of chronic muscle use and disuse on cardiolipin metabolism. *Journal of Applied Physiology.* (In press, 2013, JAPPL-01312-2012R1).

3. O'Leary MFN, Vainshtein A, Iqbal S, **Ostojic O** and Hood DA. Adaptive plasticity of autophagic proteins to denervation in aging skeletal muscle. *American Journal of Physiology-Cell Physiology.* (In press, 2013, C-00240-2012R2).

2. Iqbal S, **Ostojic O**, Singh K, Joseph AM, and Hood DA. Expression of Mitochondrial Fission and Fusion Regulatory Proteins in Skeletal Muscle during Chronic Use and Disuse. *Muscle and Nerve.* (Submitted, October 2012, MUS-12-0731).

1. O'Leary MFN, Vainshtein A, Iqbal S, Menzies KJ, **Ostojic O,** Pastore SF and Hood DA. The effects of chronic contractile activity on autophagy protein expression in young and aged skeletal muscle. (In preparation).

Book Chapter

1. Hood DA, **Ostojic O,** Saleem A, Carter HN, Vainshtein A and Iqbal S. Exercise Physiology in Canada. Textbook Chapter 14: Molecular basis of exercise training adaptations in skeletal muscle. MacIntosh BM (Editor). McGraw-Hill (Submitted August 2012).

Abstracts

6. Carter HN, O'Leary MFN, **Ostojic O***, Iqbal S*, Vainshtein A*, Pastore SF and Hood DA. Profiling Mitochondrial Turnover in Aged Skeletal Muscle: Mitophagy Arrested? *Proc. Muscle Health Awareness Day, p. 9, 2012.* *These authors made equal contributions to this work

5. **Ostojic O** and Hood DA. Cardiolipin Metabolism in Muscle. *York University Kinesiology Seminar (Oral Presentation).*

4. **Ostojic O** and Hood DA. Expression of Cardiolipin Metabolism Enzymes During Chronic Muscle Use and Disuse. *Appl. Physiol. Nutr. Metab., 36(S2): S343, 2011.*

3. Hood DA, Carter HN, **Ostojic O,** Zhang Y and Vainshtein A. The Effects of Exercise on Mitochondrial Biogenesis in Muscle. *Proc. United Mitochondrial Disease Foundation, p. 52, 2011.*

2. **Ostojic O** and Hood DA. Effects of Chronic Muscle Use and Disuse on Cardiolipin Metabolism. *Proc. Muscle Health Awareness Day, p. 23, 2011.*

1. **Ostojic O** and Hood DA. Effects of Chronic Muscle Use and Disuse on Cardiolipin Metabolism. *Proc. Ont. Exerc. Physiol. Meeting, p. 22, 2011.*